Properties of the RF transmission line of a C-shaped waveguide

Masaru Sawamura, Masato Egi, Kazuhiro Enami, Takaaki Furuya, Hiroshi Sakai, Kensei Umemori

PII: S0168-9002(17)31037-9
DOI: https://doi.org/10.1016/j.nima.2017.09.067
Reference: NIMA 60146

To appear in: *Nuclear Inst. and Methods in Physics Research, A*

Received date : 9 August 2017
Revised date : 29 September 2017
Accepted date : 29 September 2017

Please cite this article as: M. Sawamura, M. Egi, K. Enami, T. Furuya, H. Sakai, K. Umemori, Properties of the RF transmission line of a C-shaped waveguide, *Nuclear Inst. and Methods in Physics Research, A* (2017), https://doi.org/10.1016/j.nima.2017.09.067

Properties of the RF transmission line of a C-shaped waveguide

Masaru Sawamura [a,*], Masato Egi [b], Kazuhiro Enami [b],
Takaaki Furuya [b], Hiroshi Sakai [b], Kensei Umemori [b]

[a] National Institutes for Quantum and Radiological Science and Technology, Tokai, Ibaraki, 319-1106, Japan
[b] High Energy Accelerator Research Organization (KEK), Tsukuba, Ibaraki 305-0801, Japan

* Corresponding author. E-mail address: sawamura.masaru@qst.go.jp

Abstract

A new type of waveguide, named the C-shaped waveguide (CSWG), has a structure similar to that of a coaxial line but with a plate connecting the inner conductor to the outer conductor. The CSWG has unique characteristics, such as a cutoff frequency and easy cooling of the inner conductor, that are absent in the coaxial line. The results of calculations using 3-dimensional simulation software and measurement with the CSWG model are in good agreement with the analytical solution. The CSWG can be applied to a pickup port with a high-pass filter that can attenuate the higher-order modes over the cutoff frequency without attenuating the accelerating mode.

Keywords
Waveguide, Cutoff frequency, High-pass filter, Coupler

1. Introduction

Waveguides are used to transmit RF power. There are many types of waveguides, which can be classified based on their structure, e.g., rectangular, circular, coaxial, elliptical, radial, or conical. In certain waveguides, such as the rectangular waveguide (RWG) and the circular waveguide (CWG), only an outside conductor is present. Other waveguides, such as the coaxial waveguide, have both an outer conductor and an inner conductor. The RWG is used for high-power RF transmission because it is straightforward to cool this waveguide by adding a cooling path outside of the structure. Since the RWG and the CWG have a cutoff frequency, they can be used as high-pass filters. The size of the RWG is up to half of the cutoff wavelength. Many types of RF sources have a coaxial type output line requiring a converter from the coaxial to the RWG. The coaxial waveguide is also used to transmit a large amount of RF power. The coaxial waveguides have no cutoff frequency. Since the inner conductor is isolated or weakly connected through a support dielectric substance, such as Teflon, a complex system is required to cool the inner conductor. Poor cooling of the inner conductor can cause a severe problem in the case of the superconducting accelerator. The superconducting cavity has a large quality factor, giving rise to low loss of the RF power. This low loss is beneficial for the accelerating mode yet harmful for the other modes. The high Q-values of the higher-order modes (HOMs) cause beam breakup (BBU) and limit the maximum beam current [1]. Therefore, HOM damping equipment such as an HOM coupler is installed in the superconducting cavity. For high-power HOM, the inner conductor of the RF connector for HOM power extraction can lead to a temperature rise due to the weaker heat transmission from the inner conductor to the outer conductor. In the worst case scenario, an increase in the temperature of the connector leads to the quenching of superconductivity. Thus, the cooling of the inner conductor is one of the most important issues for the superconducting accelerator in continuous-wave (CW)-mode operation, such as an energy-recovery linac (ERL) [2-4].

Here, we propose a new type of waveguide. Even though the structure of this waveguide is similar to the coaxial line, it features a cutoff frequency, easy cooling, and easy connection to the coaxial waveguide. This waveguide is named the C-shaped waveguide (CSWG) because the shape of the cross-section view is similar to that of the letter C. In this paper, we describe the fundamental RF properties, the calculation and measurement results and the application of the CSWG transmission line.

2. C-shaped waveguide

2.1. Principal characteristics

To propagate RF power from/to a coaxial line to/from an RWG, a coaxial-waveguide converter is used, as shown in Fig. 1 (top left). The CSWG can be produced by transforming the coaxial-waveguide converter topologically. Shortening the narrow side of the RWG does not change the field pattern. We round the RWG so that the wide side connected with the inner conductor of the coaxial line becomes the inside, as shown in Fig. 1 (top right). This transformation changes the narrow sidewalls into a plate that connects the inner conductor to the outer conductor. Moving the coaxial line to the end of the waveguide makes the coaxial-waveguide converter to the coaxial-like line for which the inner and outer conductors are partially connected to the connection plate, as shown in Fig. 1 (bottom left). Since the part with the connection plate is originally the RWG, the properties of this part are similar to those of the RWG.

The CSWG consists of the inner conductor, the outer conductor, and the connection plate. Two types of connection plates can be considered. The first is a parallel plate, and the second is a radial plate, as shown in Fig. 2. Although the parallel plate features a simple design, its shape cannot be described using cylindrical coordinates. The radial plate enables the description of the CSWG shape using the cylindrical coordinate, enabling straightforward analysis of the electromagnetic field in the CSWG.

Here, a uniform CSWG carrying a traveling wave is considered. Field patterns inside the waveguide can be analytically investigated using Maxwell's equations when the waveguide structure is expressed in the cylindrical coordinate system. Let us consider the CSWG with an inner radius a, an outer radius b and a connection plate angle ϕ_0 that lies along the z-axis and is carrying a traveling wave in the positive z-direction, as shown in Fig. 2. The waveguide has the wall of a perfect conductor and the hollow region of a perfect dielectric.

The general solutions for the transverse electric (TE) mode can be expressed by

$$E_r(r,\phi) = \frac{\nu}{k_c r}\left[A_1 J_\nu(k_c r) + A_2 Y_\nu(k_c r)\right]\sin(\nu\phi - \phi_c)\,, \quad (1)$$

$$E_\phi(r,\phi) = \left[A_1 J_\nu'(k_c r) + A_2 Y_\nu'(k_c r)\right]\cos(\nu\phi - \phi_c)\,, \quad (2)$$

where J_ν and Y_ν are the Bessel functions of the first and the second kind, respectively, and k_c is the eigenvalue of this field. These general solutions involve arbitrary constants A_1, A_2, ν and ϕ_c, which can be fixed with the help of the boundary conditions. Applying the boundary conditions $E_r = 0$ at $\phi = \phi_0$, $2\pi\text{-}\phi_0$ gives

$$\nu = \frac{n\pi}{2(\pi - \phi_0)}\,, \quad (3)$$

where n is an integer (called the mode number and representing the mode order). In this paper, we consider the fundamental mode so that the mode number n is set to unity. Applying the boundary conditions $E_\phi = 0$ at $r = a,\ b$ gives

$$J_\nu'(k_c a)Y_\nu'(k_c b) - J_\nu'(k_c b)Y_\nu'(k_c a) = 0\,, \quad (4)$$

$$J_\nu'(k_c b\cdot\frac{a}{b})Y_\nu'(k_c b) - J_\nu'(k_c b)Y_\nu'(k_c b\cdot\frac{a}{b}) = 0\,. \quad (4)'$$

CSWGs with similar cross-sectional shapes, corresponding to the same values of a/b and ν (ϕ_0), have the same values of $k_c b$. Therefore, the eigenvalue multiplied by the outer radius, $k_c b$, is defined as the normalized eigenvalue. This equation cannot be solved analytically; Figure 3 shows the numerical solution of the normalized eigenvalue as a function of a/b and ϕ_0.

The normalized eigenvalue can be approximately expressed [5] as

$$k_c b \approx \frac{2\nu}{a+b}b = \frac{2\nu}{\frac{a}{b}+1}\,. \quad (5)$$

When the electromagnetic field has an eigenvalue, a cutoff frequency exists for the propagation through the waveguide, and the cutoff wavelength can be expressed as

$$\lambda_c = \frac{2\pi}{k_c} = \frac{2\pi}{k_c b}b \approx \frac{\pi(a+b)}{\nu} = 2\times\frac{\pi-\phi_0}{\pi}\times\pi(a+b)\,. \quad (6)$$

When the connection plate angle and the ratio of the inner radius to the outer radius are the same, the cutoff wavelength is proportional to the outer radius because the normalized eigenvalue is the same. The approximate cutoff wavelength of the CSWG can be considered to correspond to the mean circumference multiplied by two.

The approximate cutoff frequency is given by

$$f_c = \frac{c}{\lambda_c} \approx \frac{c\nu}{\pi(a+b)}\,, \quad (7)$$

where c is the velocity of light.

2.2. Calculation and measurement

To confirm the CSWG properties, calculations using a simulation code and measurements using a

CSWG model were performed. The calculations were performed using the 3-dimensional RF simulation software CST MW-Studio. The CSWG model was fabricated as shown in Fig. 4. The CSWG model consisted of the inner conductor, the outer conductor, and the connection plate. The radius of the outer conductor was fixed to 21 mm, and that of the inner conductor varied, as shown in Table 1. The CSWG model was connected to the coaxial-N-type-connector converter. Since the coaxial-N-type-connector has an outer diameter of 38.8 mm and an inner diameter of 16.9 mm, a tapered coaxial line with a length of 33 mm was installed between the CSWG and the coaxial-N-type-connector. The calculation model also included the tapered coaxial lines. The combination of four CSWG models with different lengths caused the total length to vary from 65 mm to 560 mm.

Figure 5 shows the calculated and measured results for the transmission properties of the CSWG and the coaxial line. The models for the calculation and measurement had an inner radius of 9 mm, and the outer radius was 21 mm for the coaxial line and the CSWG. The CSWG contained a parallel connection plate with a thickness and length of 2 mm and 560 mm, respectively. The coaxial line showed no transmission attenuation. While the transmission of the CSWG above 1.7 GHz was similar to that of the coaxial line, the transmission strength below 1.7 GHz decreased with a decreasing frequency, indicating that the CSWG has a cutoff frequency. The measured results were in agreement with the results of the calculation.

Figure 6 shows the measured and calculated transmission coefficients through the CSWG for the radial connection plate with different angles of 15, 30, 45, and 60 degrees. The cutoff frequency increases with the increasing angle of the radial connection plate.

Figure 7 shows the measured and calculated transmission coefficients through the CSWG for the parallel connection plate with different inner conductor radii of 4.5, 6, 7.5, 9, and 15 mm. The cutoff frequency decreases with the increasing radius of the inner conductor.

Figure 8 shows the measured and calculated transmission coefficients through the CSWG for the parallel connection plate and the inner radius of 9 mm with the length varying from 65 mm to 560 mm. As the CSWG length increases, the attenuation below the cutoff frequency becomes steeper.

2.3. Comparison of cutoff frequency

Since the calculated and measured transmission around the cutoff frequency is not sufficiently sharp for the direct evaluation of the cutoff frequency, the cutoff frequency is determined by fitting the attenuation curve below the cutoff frequency. The transmission coefficient S_{21} can be expressed using the attenuation constant α and length z as

$$S_{21} = e^{-2\alpha z}. \qquad (8)$$

The attenuation constant can be expressed as

$$\alpha = \sqrt{k_c^2 - k^2} = \frac{2\pi}{c}\sqrt{f_c^2 - f^2}\,. \qquad (9)$$

Since the transmission coefficient can be expressed as a function of f with the constants f_c and z, fitting of the attenuation curve enables the determination of the cutoff frequency.

Table 2 shows a comparison of the cutoff frequencies of the radial connection plate determined by the analysis, measurement, calculation, and approximation. The measurement and calculation results are in good agreement with the analysis results, and the approximated values are a few percent lower than the analysis values.

Since the cutoff frequency for the parallel connection plate cannot be derived analytically, we consider the differences obtained by the calculations. Figure 9 shows the calculated solution of the normalized eigenvalue for the parallel connection plate as functions of a/b and t/b. Table 3 shows the comparison of the cutoff frequency obtained in the measurements and those obtained using the approximation. The measured values are in good agreement with the calculation results. The approximation values are larger than the calculation values, and the smaller inner radius shows a larger error relative to the calculation.

The above approximation used the average radius for the circumference. The arrows in Figure 10 show the electric field in the CSWG with the radial connection plate, $a/b = 0.43$ and $\phi_0 = 14°$. The blue broken line and the red solid line show the average radius and the radial position of the average field at an angle ϕ, respectively. Most of the radial position of the average field is inside of the average radius.

Here, we use the radius position fraction s from the inner radius to outer radius. A value of s equal to 0 corresponds to the inner radius, and 0.5 corresponds to the average radius. In Figure 10 case, a value of s for the radial position of the average field at an angle ϕ varies from 0.427 to 0.703. The minimum value of s occurs where the average field is maximum, and the average of s in the CSWG is 0.469.

Using the radial position fraction, the approximation for the normalized eigenvalue can be expressed as

$$k_c b = \frac{\nu}{(1-s)\frac{a}{b} + s}. \tag{10}$$

Figure 11 (left) shows the approximation error of the cutoff frequency from the numerical solution for the radial connection plate as functions of a/b and ϕ_0 for s equal to 0.5. The error due to ϕ_0 is small, and the lower value of a/b increases the error. For a/b greater than 0.3, the error is less than 6% for the practical connection plate angle values. Figure 12 (left) also shows the approximation error of the cutoff frequency from the calculation for the parallel connection plate as functions of a/b and t/b for s equal to 0.5.

Since the position of the average field is closer to the inner conductor than the average radius, the use of the radius at the position fraction of 0.45 instead of the average radius reduces the error to smaller than 2% for both the radial and the parallel connection plates in a wide range of angles, as shown in Figs. 11 (right) and 12 (right). The position fraction of 0.45 is consistent since the characteristic radius can be thought to be between the minimum value of the maximum average field and the unweighted average value of the average field.

2.4. Connecting CSWGs

When coaxial lines are connected, an inner conductor tube and an outer conductor tube are used. The inner and the outer conductor tubes can similarly be used for connecting the inner and the outer conductors of CSWGs. The connection of the connection plate must be considered. One connection method is to insert a metal sheet between the connection plate ends to obtain firm contact. In the other method, no connection of the connection plates is used. The region containing no connection plate can be assumed to be similar to the coaxial line, where the RF power can be propagated. Figure 13 shows the calculated and measured transmission coefficients through the CSWG with some missing part of the connection plate. A missing connection plate distance of less than 10 mm makes almost no difference. By contrast, while a missing connection plate distance of more than 10 mm makes only a slight difference for the frequencies above the cutoff frequency, below the cutoff frequency, peaks are observed depending on the length of the missing part of the connection plate.

2.5. Matching

The impedance of a coaxial line can be expressed as

$$Z_0 = \frac{\zeta}{2\pi} \ln \frac{b}{a}. \qquad \zeta = \sqrt{\frac{\mu}{\varepsilon}}, \qquad (11)$$

where ε is the permittivity, and μ is the permeability. The impedance of a waveguide with a cutoff frequency f_c is expressed as

$$Z_0 = \frac{\zeta}{\sqrt{1-\left(\frac{f_c}{f}\right)^2}}. \qquad (12)$$

The impedance of the coaxial line is determined by the ratio of the inner and the outer radii, and that of the waveguide proposed here varies with the ratio between the frequency and the cutoff frequency. The impedance of the coaxial line is approximately 2π times smaller than that of the waveguide. Simply connecting the CSWG to the coaxial line gives rise to an impedance gap between the coaxial line and the CSWG and results in reflection and loss, as shown in Fig. 14.

Since it is impossible to achieve impedance matching in the entire frequency range, a certain band will be considered. An aperture at the RF window has been used previously to match the impedance between a cavity and a transmission line. A similar structure was applied here for CSWGs. A disk with the radius larger than that of the inner conductor is placed between the coaxial line and the CSWG. Furthermore, the impedance of the coaxial line component can be increased by increasing the radius of the outer conductor and decreasing the radius of the inner conductor. Figure 15 shows the schematics of matching sections with the disk using the larger outer conductor and the smaller inner conductor. Figures 16 and 17 show the calculated and measured transmission and reflection coefficients. The radii of the outer and inner conductors were 21 and 9 mm, respectively, and the thickness of the parallel connection plate was 2 mm for the CSWG component. Figure 16 shows the results with the inner conductor radii of 6, 7.5 and 9 mm for the matching section. The outer radius was 21 mm, and the disk radius was 13 mm. These results indicate that the matching section improves the transmission and that the larger inner radius shifts the flat region of the transmission coefficients to higher frequencies. Figure 17 shows the result for the larger outer conductor radii of 35 mm and 40 mm for the matching section. The inner radius was 9 mm, and the disk radius was 13 mm. These results show favorable matching at approximately 2.1 GHz.

3. Applications

3.1. Coupling models

One of the applications of CSWG is a pickup port with a high-pass filter used for HOM couplers. The TESLA-type HOM coupler has an isolated or weakly connected inner conductor, which tends to cause problematic heating in the extraction of the high-power HOMs. By contrast, cooling is straightforward for the CSWG because of the strong connection of the inner conductor to the outer conductor. Furthermore, the TESLA-type HOM coupler requires adjustment to tune the filter, and cooling to liquid-helium temperatures tends to shift the tuning. By contrast, the CSWG requires no tuning because the cutoff frequency is determined by the shape of the CSWG cross section. However, the CSWG requires a long waveguide to avoid damping the fundamental mode similar to the waveguide-type HOM damper using the RWG [6].

To evaluate the feasibility, the CSWG pickup model was fabricated as shown in Fig. 18. The CSWG was installed at the center of the coaxial transmission line [7]. The RF transmission and reflection coefficients were measured using the three ports. Two ports were connected to the network analyzer, and the other port was terminated with a dummy load. The two ports of the coaxial transmission line were numbered 1 and 2, and the CSWG port was numbered 3. To compare to the coaxial line pickup port, the coaxial line was also installed instead of the CSWG. The outer and inner radii were 21 mm and 9 mm, respectively. The CSWG has a parallel connection plate with a thickness of 2 mm. The cutoff frequency was 1.7 GHz. Figure 19 shows the measurement results of transmission coefficient from the coaxial transmission line through the CSWG and the coaxial line (S_{31}) (left) and transmission coefficient through the coaxial transmission line (S_{21}) (right). The S_{21} of the coaxial line is almost identical to that of the CSWG. The S_{31} value of the CSWG decreases below the cutoff frequency of 1.7 GHz and above the cutoff frequency, but the obtained values are almost the same as those of the coaxial line.

3.2. Coupling properties

To check the coupling properties, the RF transmission coefficients were measured for the different CSWG parameters. Figure 20 shows the S_{31} transmission coefficients for the various CSWG lengths. Longer CSWGs show steeper attenuation below the cutoff frequency. Figure 21 shows the S_{31} transmission coefficients for the tip position of the CSWG. It is clear that a deeper tip in the coaxial transmission line causes stronger coupling. Figure 22 shows the S_{31} transmission coefficients by changing the direction of rotation of the connection plate, revealing that the direction of rotation of the connection plate makes no difference.

3.3. Peak properties

The peaks appear below the cutoff frequency as observed in Figs. 20-22. While the CSWG length does not affect peak frequencies, tip length changes do lead to changes in the peak frequencies. These peaks occur due to the resonance near the CSWG tip. Figure 23 shows the electric fields at the frequencies away from and at the peak. At frequencies away from the peak, some power is transmitted through the coaxial transmission line, and some is transmitted through the CSWG, as shown in Fig. 23 (left). At the peak frequency, the tip and the CSWG behave as a quarter-wavelength resonator, as shown in Fig. 23 (right). The peak frequencies were calculated for different tip lengths and cutoff frequencies. Figure 24 shows the peak frequency as a function of the tip length. The tip length is normalized using the wavelength of the peak, and the peak frequency is normalized using the cutoff frequency. By normalizing by the cutoff frequency and the wavelength, the peak frequency can be described using a single curve. The curve can be explained as follows.

(1) When the peak frequency is much lower than the cutoff frequency (corresponding to f_p/f_c approaching zero), the RF power cannot penetrate into the CSWG, and the tip length approaches the quarter wavelength of the peak.

(2) When the peak frequency approaches the cutoff frequency (corresponding to f_p/f_c approaching unity), a resonator is formed within the CSWG, and the tip is not required for resonation.

The tip length must be properly selected to not overlap the frequencies of the modes to be attenuated with the resonant modes.

4. Conclusion

A new type of transmission line CSWG was proposed. The CSWG has a similar structure to the coaxial line and shows a cutoff frequency that depends primarily on the outer and inner radii. This transmission line can be applied for pickup port couplers, such as HOM couplers for superconducting cavities. Since the CSWG features a connection plate between the inner and outer conductor, the CSWG is preferable when cooling of the inner conductor is a matter of concern for high-power transmission.

Acknowledgments

This work was supported by JSPS KAKENHI Grant Number JP15K04726.

References

[1] E. Pozdeyev *et al.*, Multipass beam breakup in energy recovery linacs, Nucl. Instrum. and Methods in Phys. Res. A 557 (2006) p. 176.

[2] P. Kneisel *et al.*, Testing of HOM Coupler Designs on a Single Cell Niobium Cavity, in *Proceedings of 2005 Particle Accelerator Conference, PAC05, Knoxville, Tennessee*, (2005) p. 4012.

[3] G. Wu *et al.*, Electromagnetic Simulations of Coaxial Type HOM Coupler, in *Proceedings of 12th International Workshop of RF Superconductivity, SRF2005, Ithaca, New York*, (2005) p.600.

[4] J. Sekutowicz, Improved Heat Conduction Feedthroughs for HOM Couplers at DESY, in *Proceedings of ERL2011, Tsukuba, Japan*, (2011) p. 102.

[5] K. A. Milton and J. Schwinger, Electromagnetic Radiation: Variational Methods, Waveguides and Accelerators, (Springer-Verlag Berlin Heidelberg, 2006) p. 153.

[6] R. Rimmer *et al.*, Concepts for the Jlab Ampere-class CW Cryomodule, in *Proceedings of 2005 Particle Accelerator Conference, PAC05, Knoxville, Tennessee*, (2005) p. 3588.

[7] K. Watanabe *et al.*, New HOM coupler design for ILC superconducting cavity, Nucl. Instrum. and Methods in Phys. Res. A 595 (2008) p. 299.

Figure Captions

Fig. 1. Transformation from a coaxial-waveguide converter (top left) to a CSWG (bottom left).

Fig. 2. Schematic CSWG cross sections with the radial connection plate (left) and the parallel connection plate (right).

Fig. 3. Numerical solution of normalized eigenvalues for the radial connection plate.

Fig. 4. CSWG model connected with coaxial-N-type-connector converters (left). Cross sections of the parallel and radial-type CSWG models (right).

Fig. 5. Measured and calculated transmission through the CSWG and the coaxial line.

Fig. 6. Measured (left) and calculated (right) transmission coefficients for the radial-type CSWG with different connection plate angles.

Fig. 7. Measured (left) and calculated (right) transmission coefficients for the parallel-type CSWG with different inner radii.

Fig. 8. Measured (left) and calculated (right) transmission coefficients for the parallel-type CSWG with different lengths.

Fig. 9. Calculated normalized eigenvalue for the parallel connection plate.

Fig. 10. Electric field (arrows), the average radius (blue broken line) and the radial position of the average field at an angle ϕ (red solid line) in the CSWG with the radial connection plate, $a/b = 0.43$ and $\phi_0 = 14°$.

Fig. 11. Approximation error of the cutoff frequency from the numerical solution for a radial connection plate as functions of a/b and ϕ_0 when the radial position fraction is equal to 0.5 (left) and 0.45 (right).

Fig. 12. Approximation error of the cutoff frequency from calculations for the parallel connection plate as functions of a/b and t/b when the radial position fraction is equal to 0.5 (left) and 0.45 (right).

Fig. 13. Calculated (top) and measured (middle) transmission and reflection coefficients through the CSWG with some missing part of the connection plate (bottom).

Fig. 14. Calculated and measured transmission and reflection coefficients without the matching section. The first number in the legend indicates the outer radius, the second indicates the inner radius, and the third indicates the disk radius of the matching section.

Fig. 15. Schematics of matching sections with the large outer conductor, the small inner conductor, and the disk.

Fig. 16. Calculated and measured transmission and reflection coefficients with the matching section. The first number in the legend indicates the outer radius, the second indicates the inner radius, and the third indicates the disk radius of the matching section.

Fig. 17. Calculated and measured transmission and reflection coefficients with the matching section. The first number in the legend indicates the outer radius, the second indicates the inner radius, and the third indicates the disk radius of the matching section.

Fig. 18. Coaxial transmission line with CSWG type pickup port (left) and schematic view (right).

Fig. 19. (left) Measured transmission coefficients from the coaxial transmission line through the two types of pickup port of CSWG and coaxial line. (right) Measured transmission coefficients through the coaxial transmission line with the two types of pickup port of CSWG and coaxial line.

Fig. 20. Measured transmission coefficients for various CSWG lengths.

Fig. 21. Measured transmission coefficients with various tip positions of the CSWG.

Fig. 22. Measured transmission coefficients with various direction of rotations of the CSWG.

Fig. 23. Electric fields of the coaxial transmission line and the CSWG (left) at the frequency away from the peak and (right) at the peak frequency.

Fig. 24. Calculated peak frequencies as a function of tip length with various cutoff frequencies of CSWGs. The tip length and peak frequency are normalized by the peak wavelength and cutoff frequency, respectively.

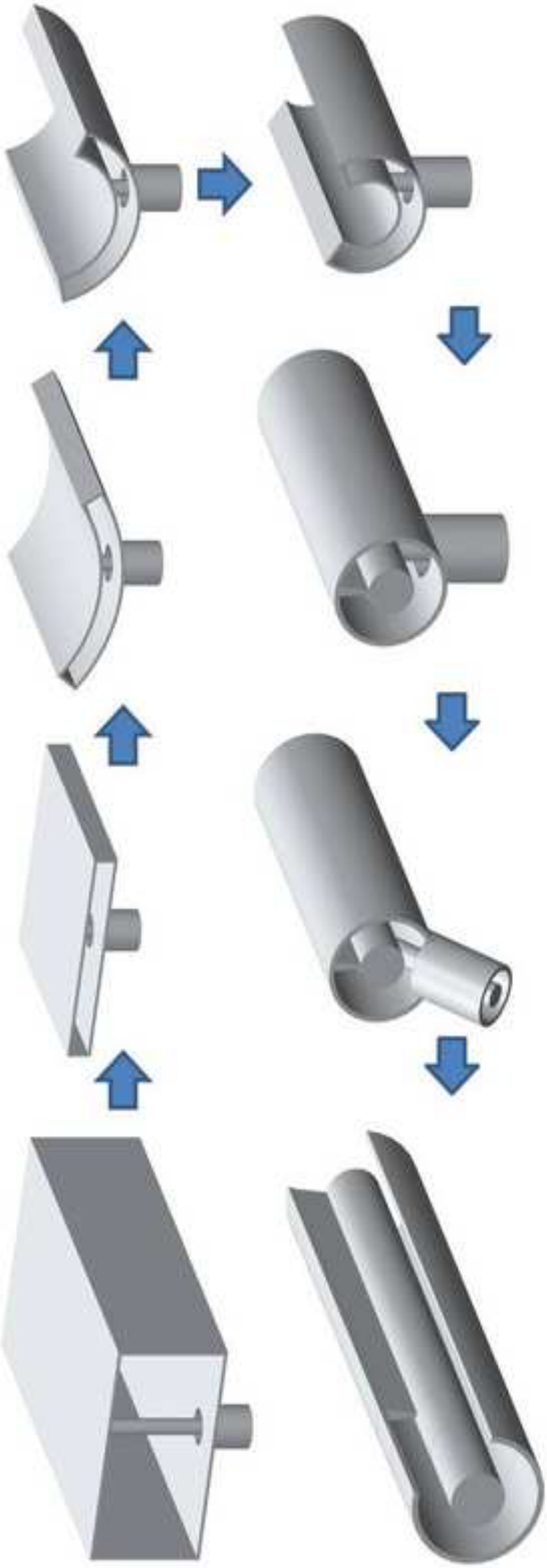

Figure

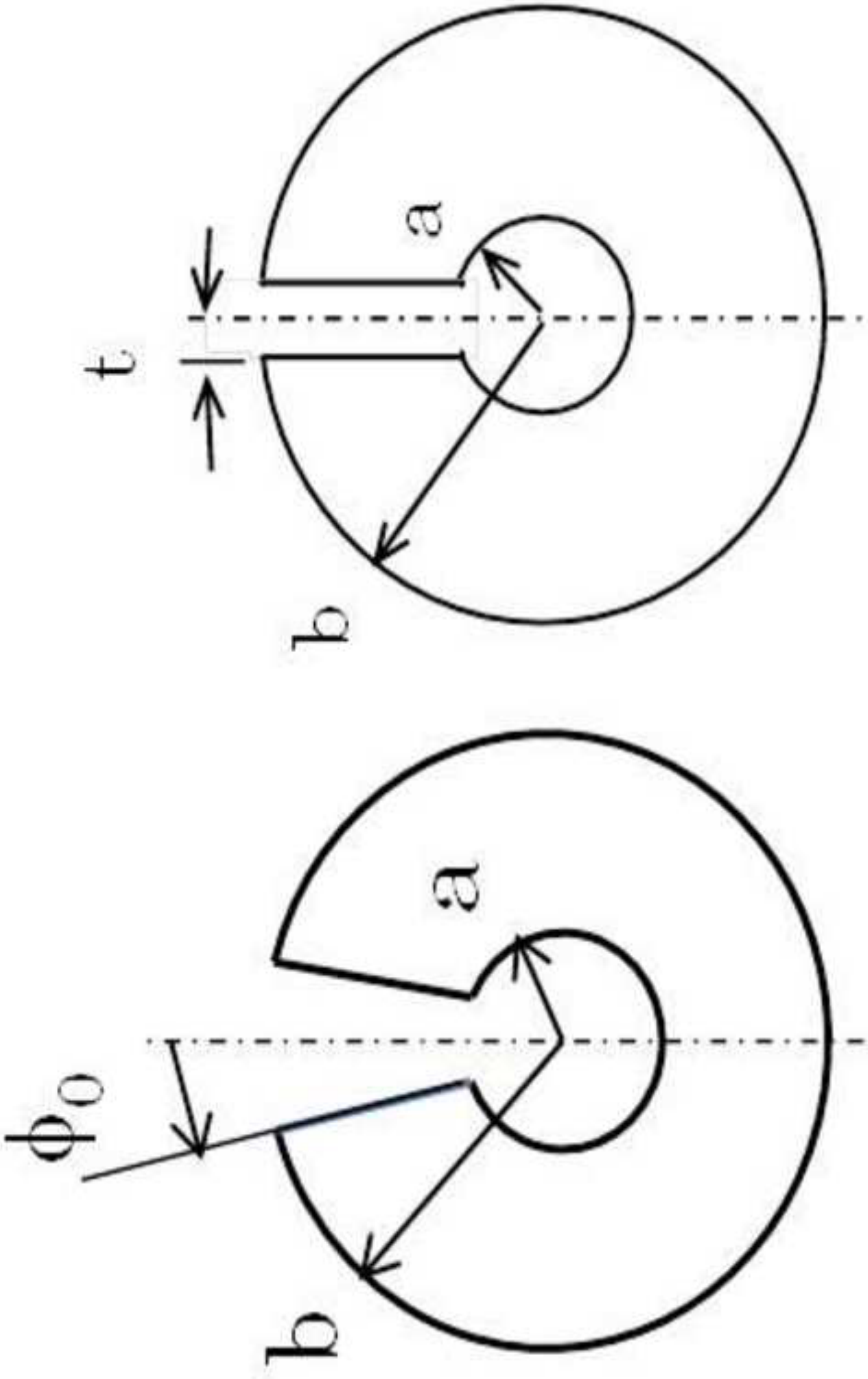

Figure

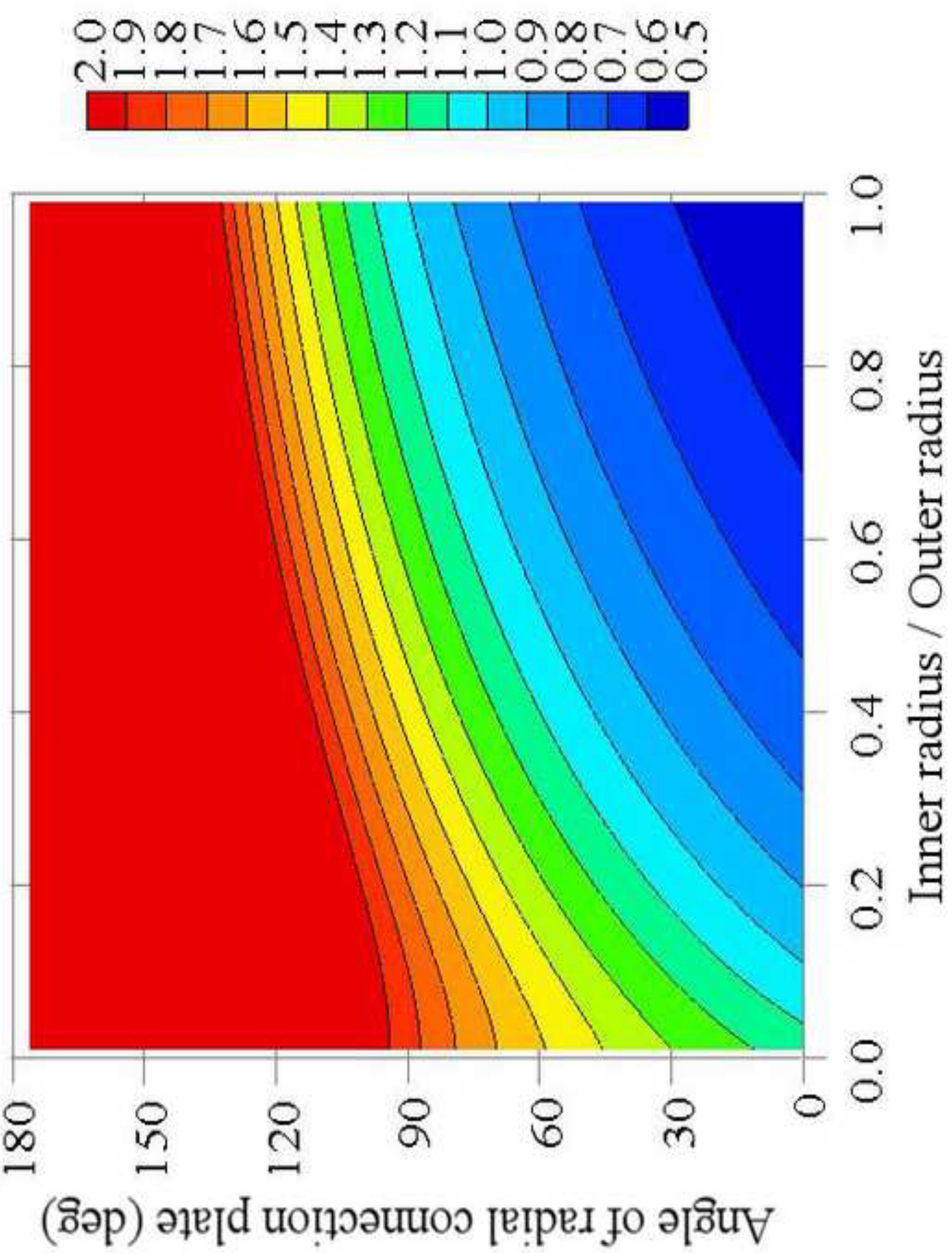

Angle of radial connection plate (deg)
180
150
120
90
60
30
0
0.0
0.2
0.4
0.6
0.8
1.0
Inner radius / Outer radius
2.0
1.9
1.8
1.7
1.6
1.5
1.4
1.3
1.2
1.1
1.0
0.9
0.8
0.7
0.6
0.5

Figure

Figure

Figure

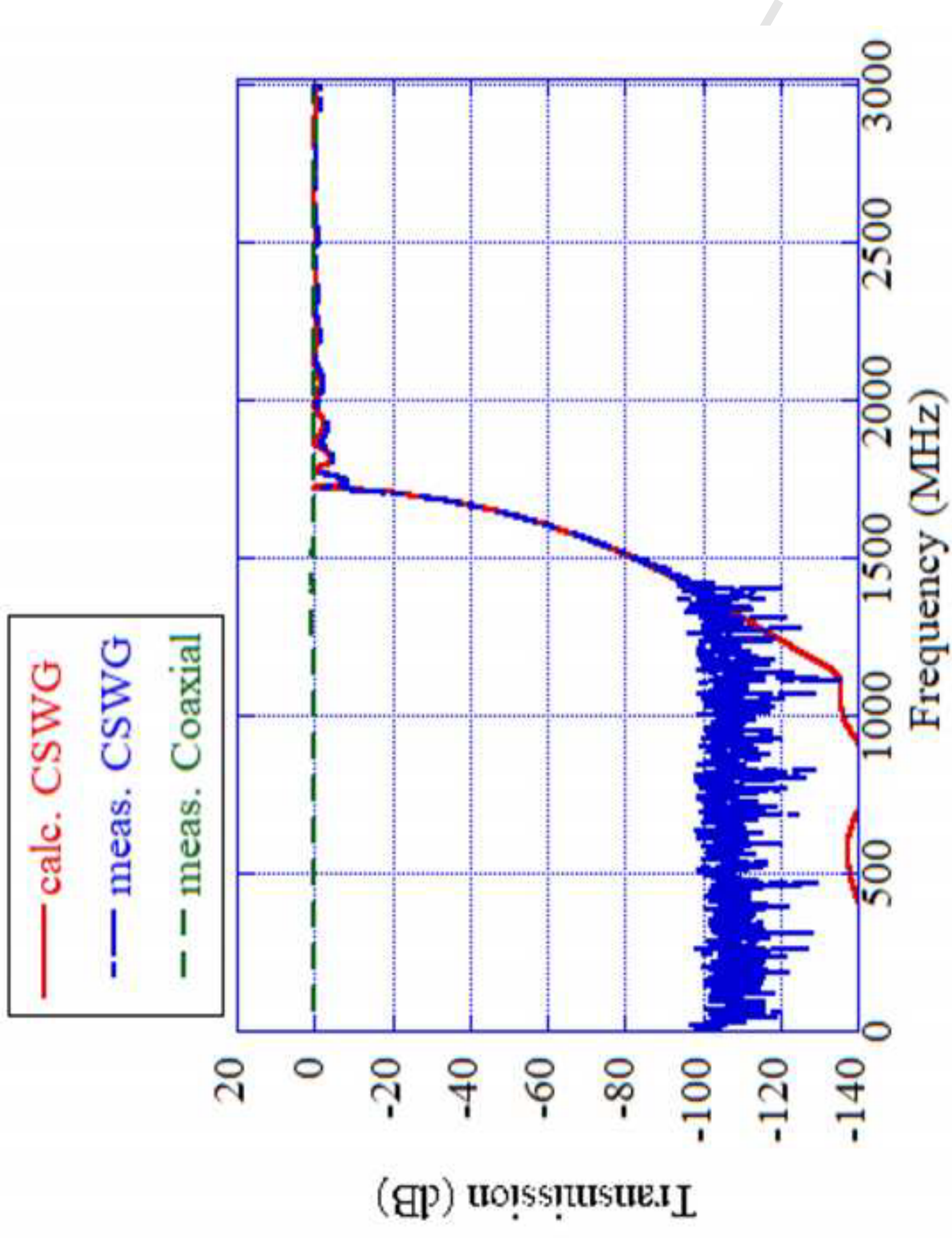

calc. CSWG
meas. CSWG
meas. Coaxial
Transmission (dB)
Frequency (MHz)
20
0
-20
-40
-60
-80
-100
-120
-140
0
500
1000
1500
2000
2500
3000

Figure

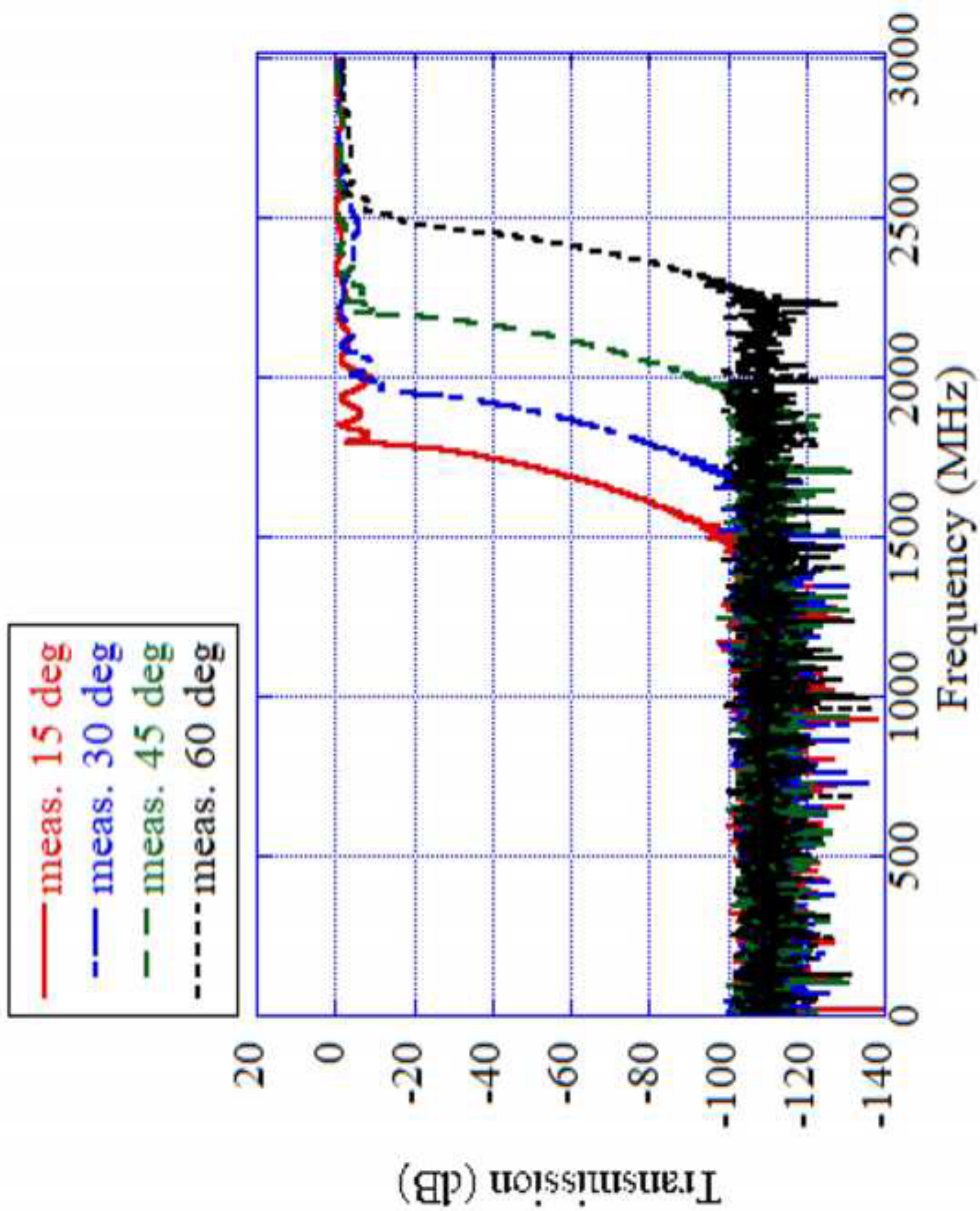

meas. 15 deg
meas. 30 deg
meas. 45 deg
meas. 60 deg
Transmission (dB)
Frequency (MHz)
20
0
-20
-40
-60
-80
-100
-120
-140
0
500
1000
1500
2000
2500
3000

Figure

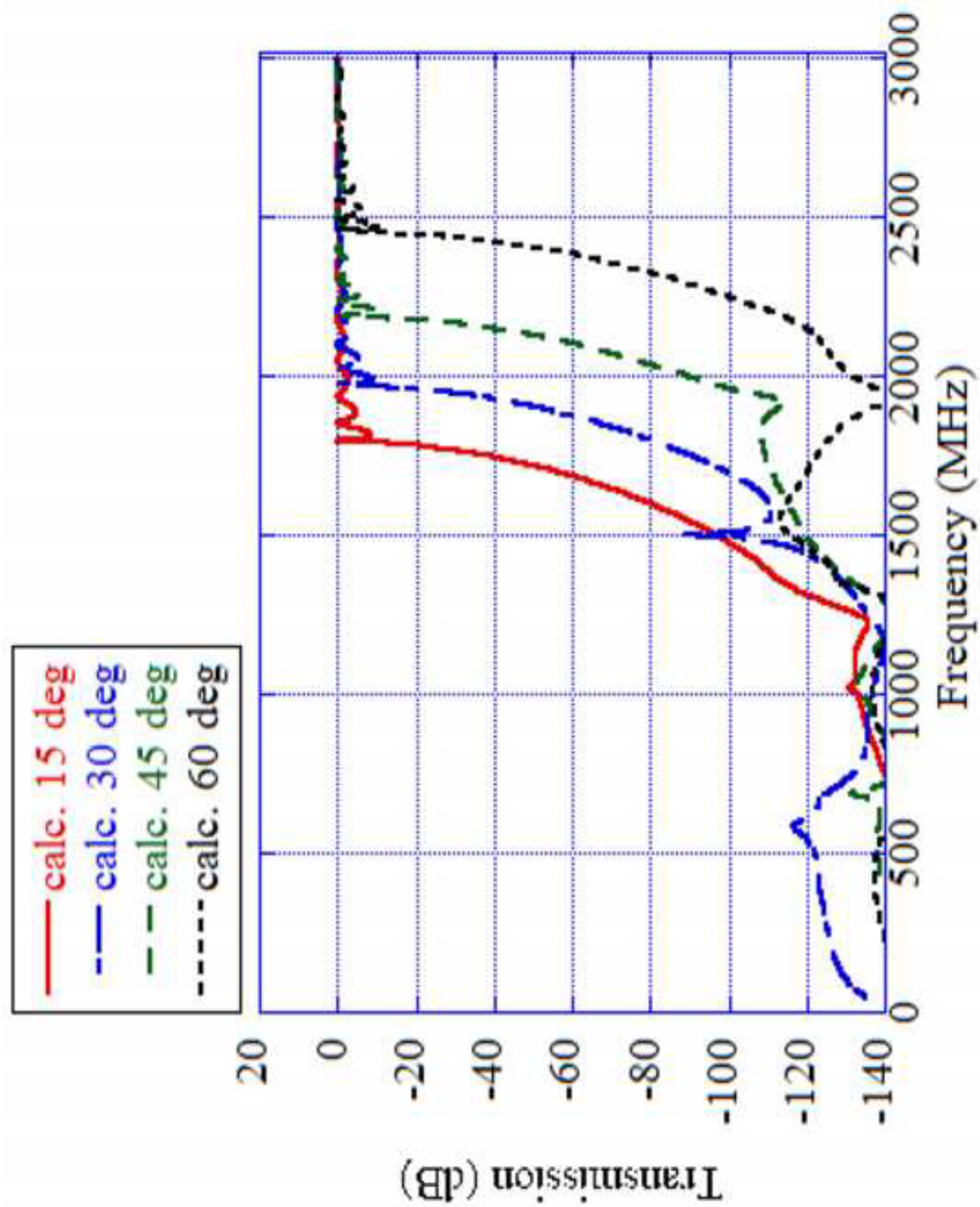

calc. 15 deg
calc. 30 deg
calc. 45 deg
calc. 60 deg
Transmission (dB)
20
0
-20
-40
-60
-80
-100
-120
-140
Frequency (MHz)
0
500
1000
1500
2000
2500
3000

Figure

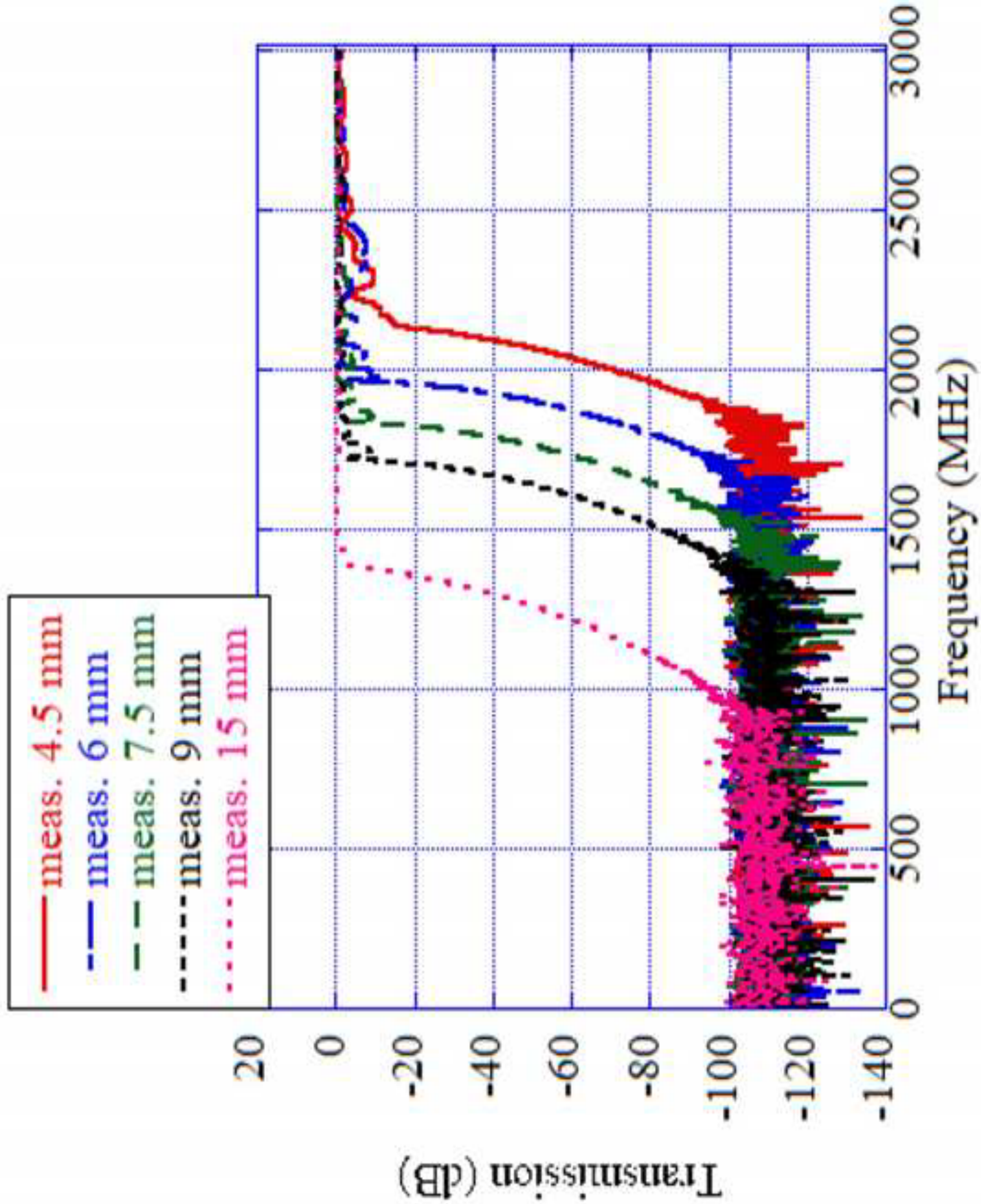
meas. 4.5 mm
meas. 6 mm
meas. 7.5 mm
meas. 9 mm
meas. 15 mm
Transmission (dB)
Frequency (MHz)
20
0
-20
-40
-60
-80
-100
-120
-140
0
500
1000
1500
2000
2500
3000

Figure

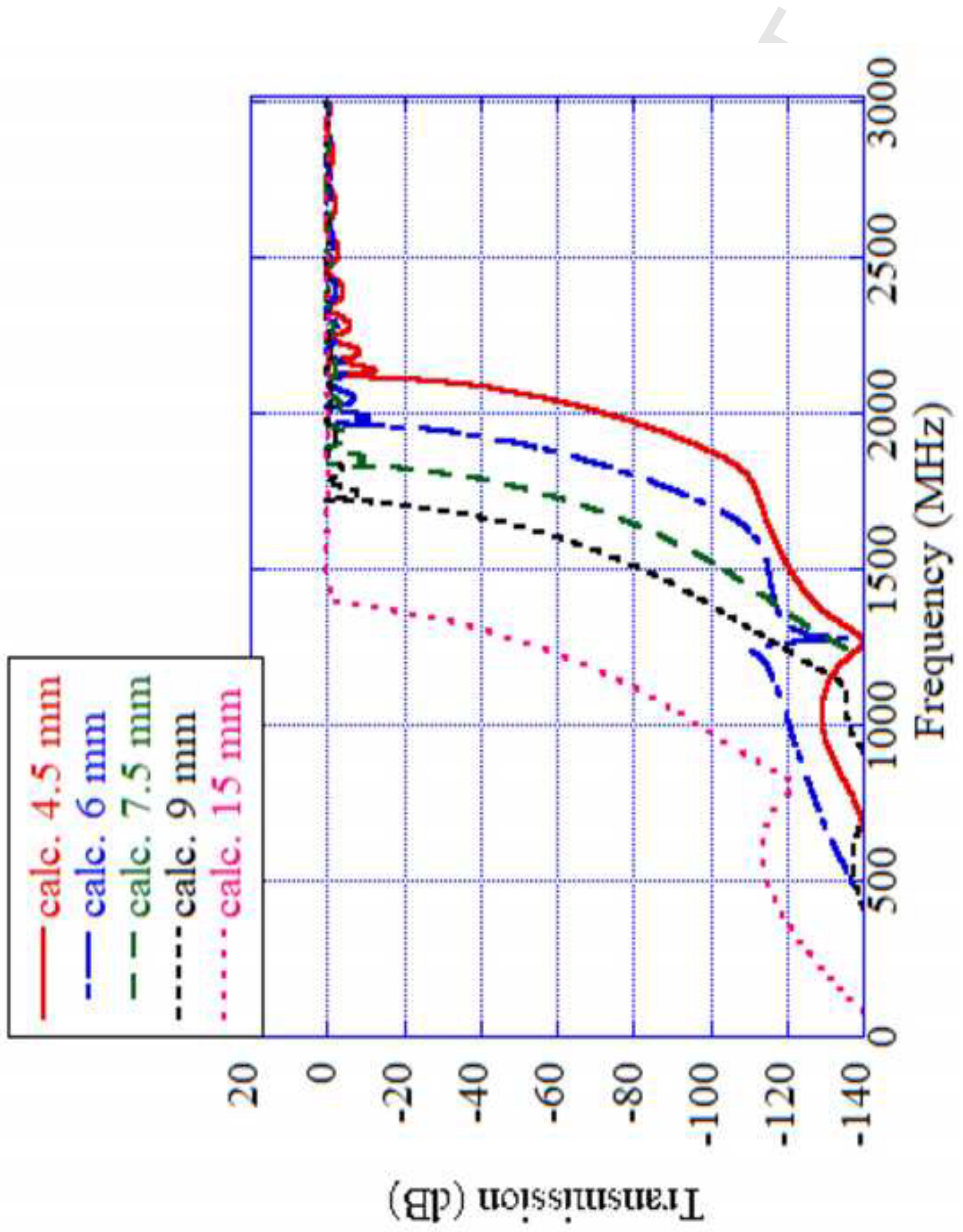
calc. 4.5 mm
calc. 6 mm
calc. 7.5 mm
calc. 9 mm
calc. 15 mm
Transmission (dB)
Frequency (MHz)
20
0
-20
-40
-60
-80
-100
-120
-140
0
500
1000
1500
2000
2500
3000

Figure

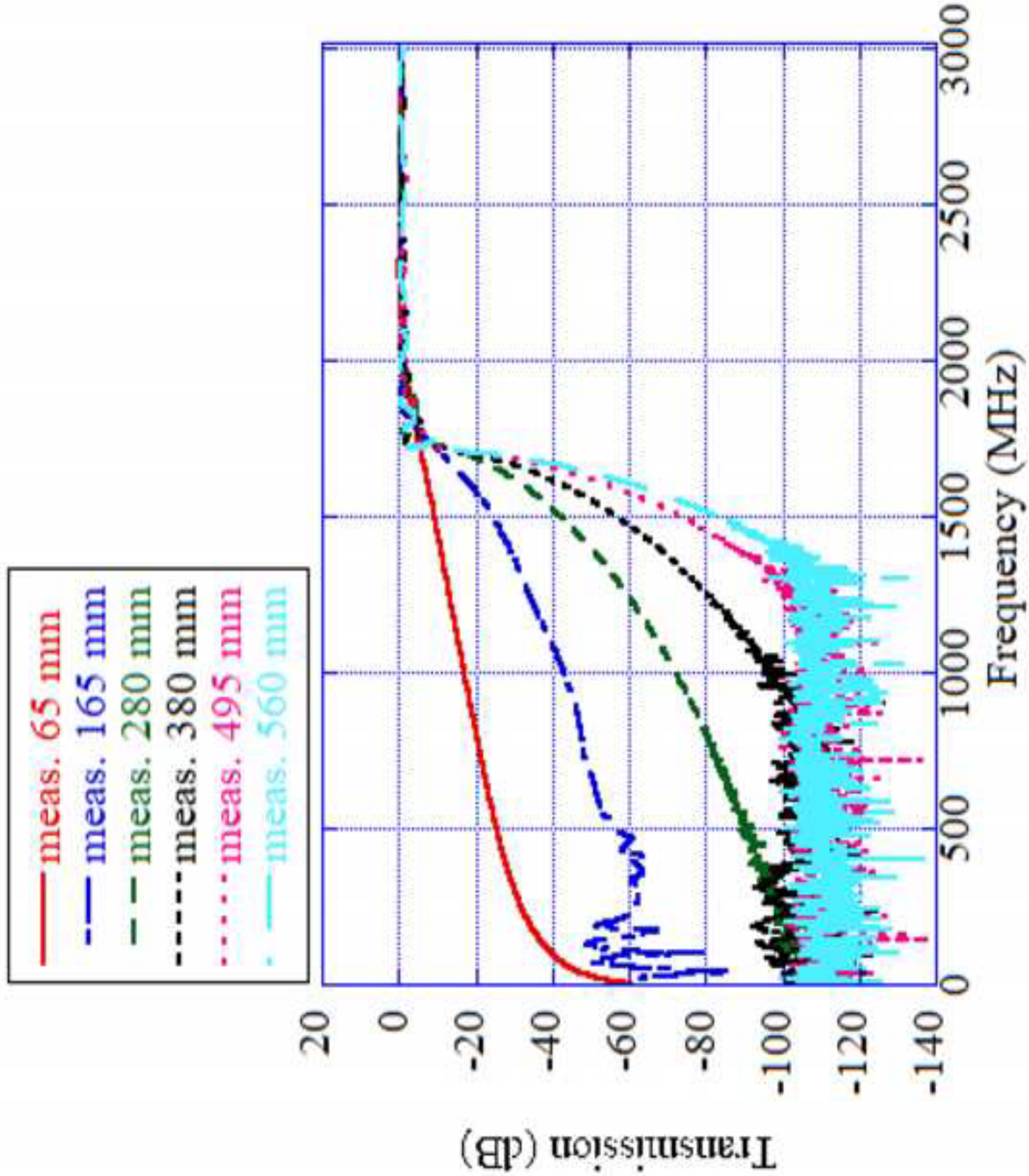

meas. 65 mm
meas. 165 mm
meas. 280 mm
meas. 380 mm
meas. 495 mm
meas. 560 mm
Transmission (dB)
20
0
-20
-40
-60
-80
-100
-120
-140
Frequency (MHz)
0
500
1000
1500
2000
2500
3000

Figure

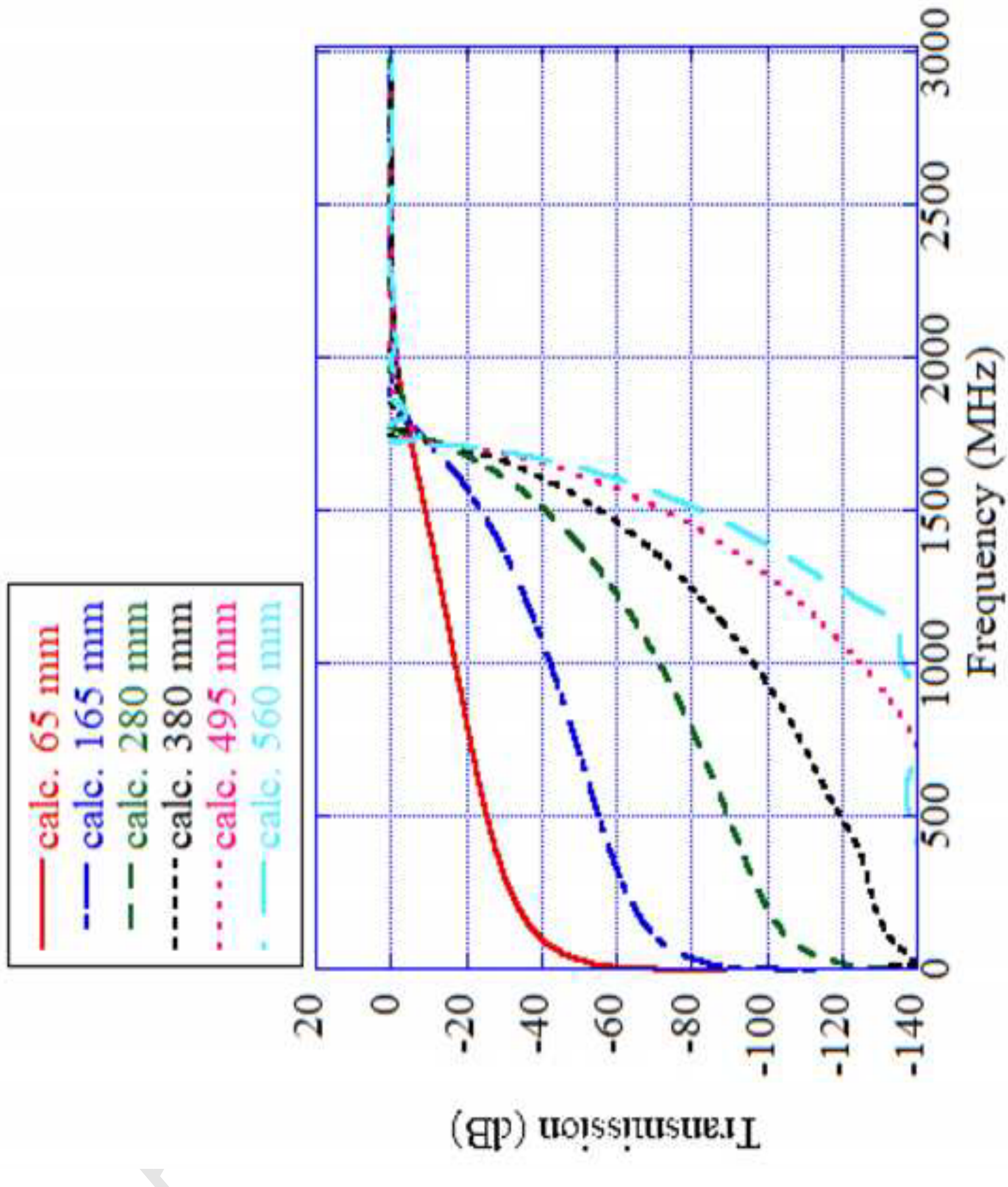
calc. 65 mm
calc. 165 mm
calc. 280 mm
calc. 380 mm
calc. 495 mm
calc. 560 mm
Transmission (dB)
20
0
-20
-40
-60
-80
-100
-120
-140
Frequency (MHz)
0
500
1000
1500
2000
2500
3000

Figure

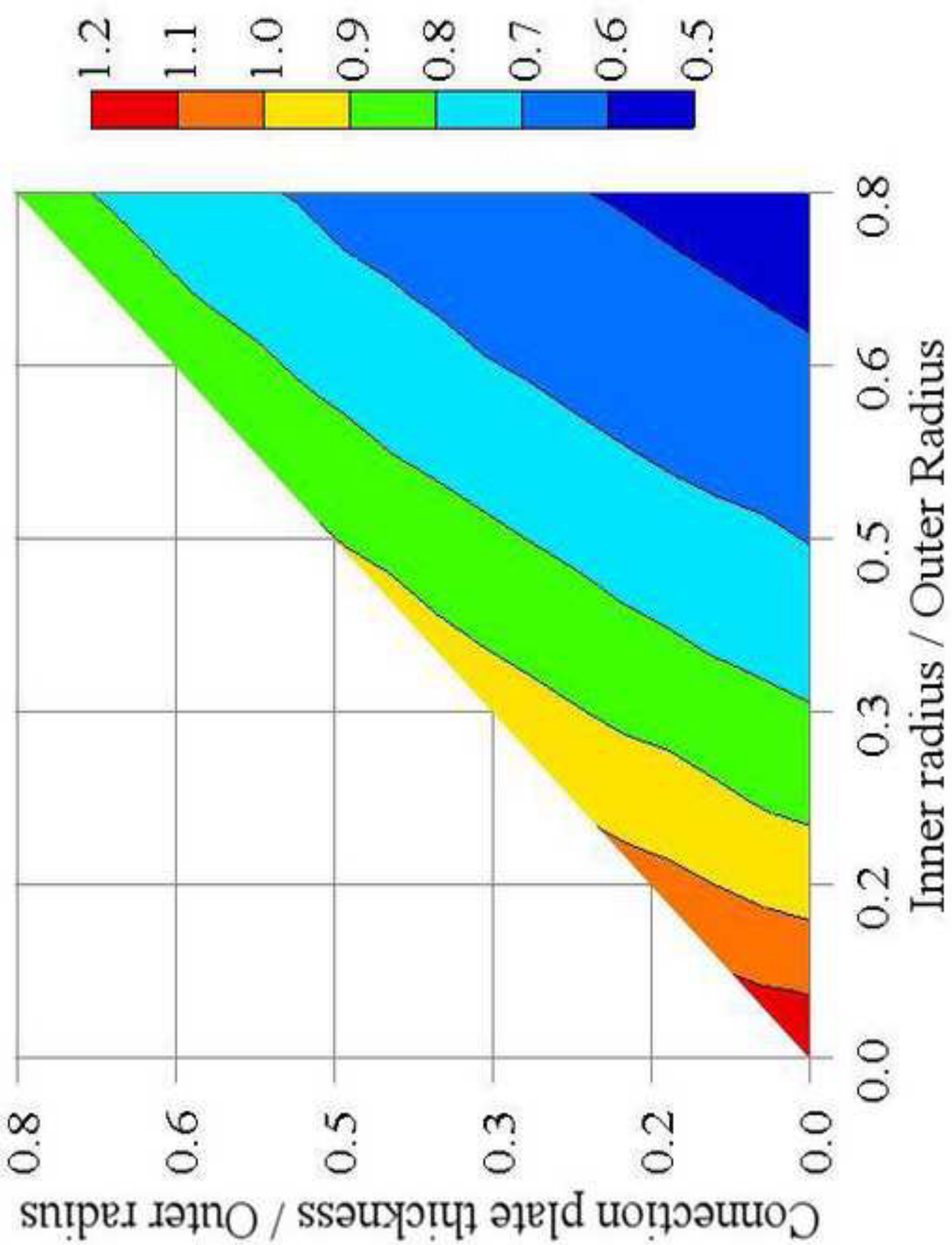

1.2
1.1
1.0
0.9
0.8
0.7
0.6
0.5
0.0
0.2
0.3
0.5
0.6
0.8
Inner radius / Outer Radius
Connection plate thickness / Outer radius

Figure

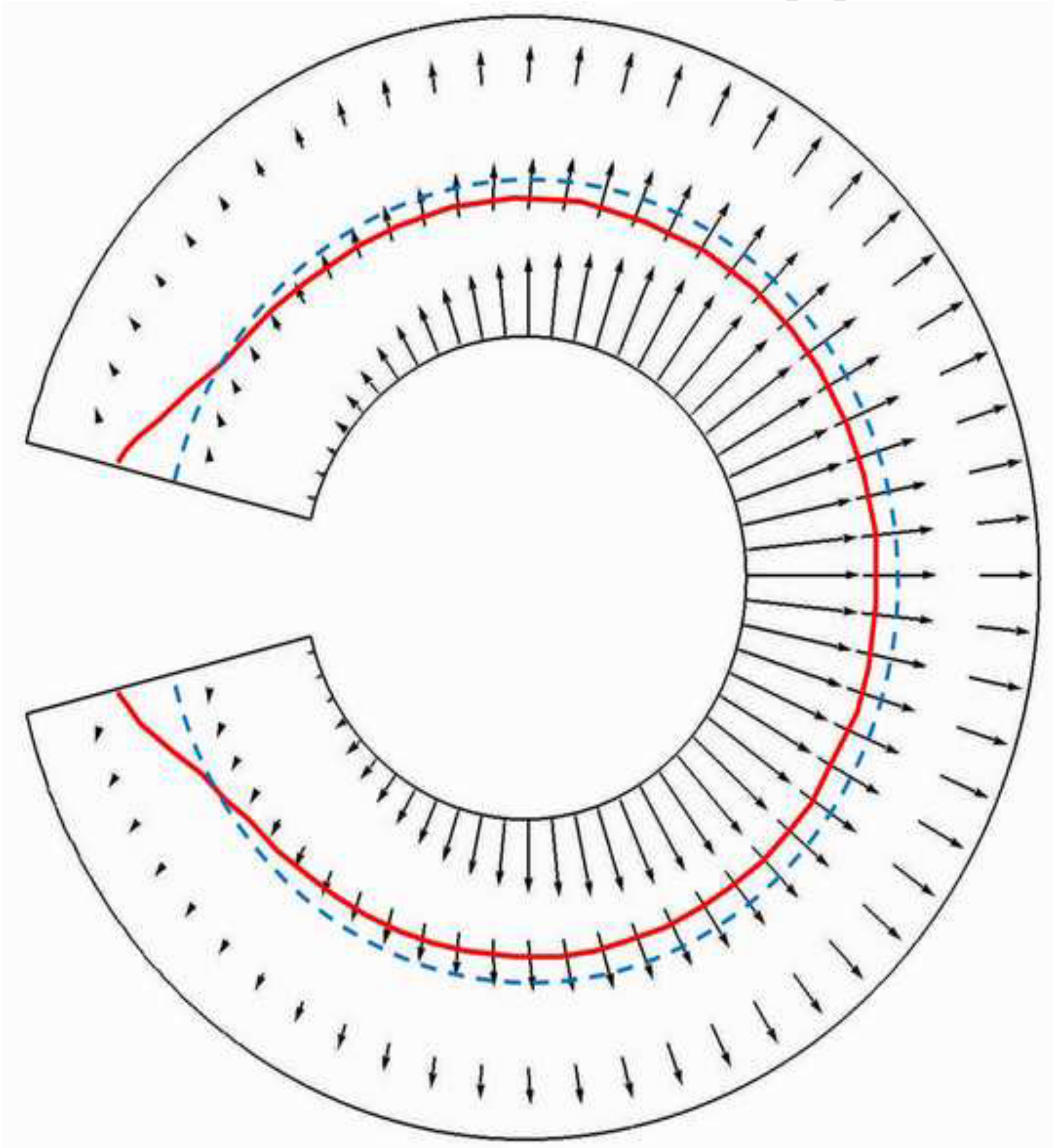

Figure

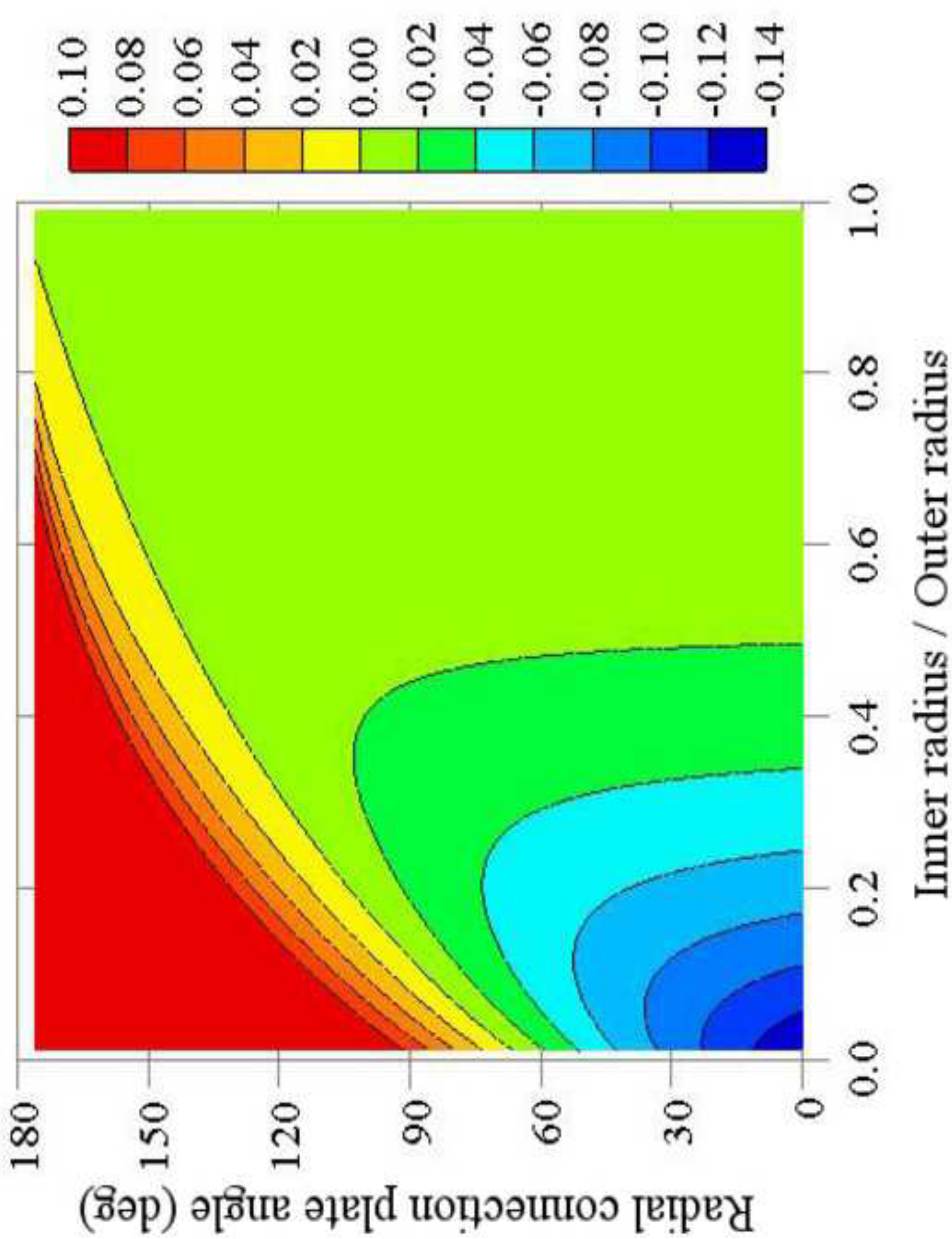

0.10
0.08
0.06
0.04
0.02
0.00
-0.02
-0.04
-0.06
-0.08
-0.10
-0.12
-0.14
Radial connection plate angle (deg)
180
150
120
90
60
30
0
0.0
0.2
0.4
0.6
0.8
1.0
Inner radius / Outer radius

Figure

Figure

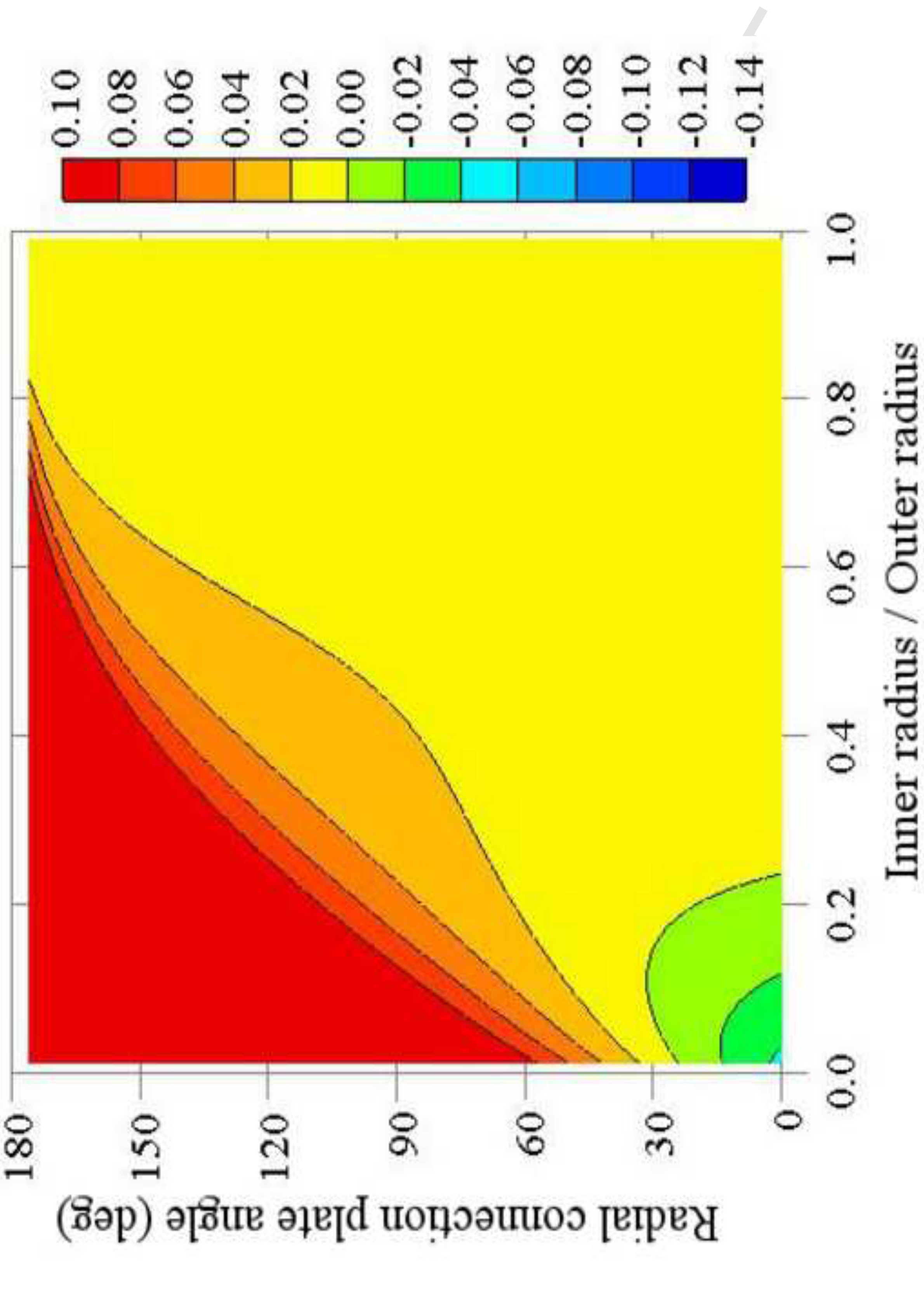
0.10
0.08
0.06
0.04
0.02
0.00
-0.02
-0.04
-0.06
-0.08
-0.10
-0.12
-0.14
Radial connection plate angle (deg)
180
150
120
90
60
30
0
0.0
0.2
0.4
0.6
0.8
1.0
Inner radius / Outer radius

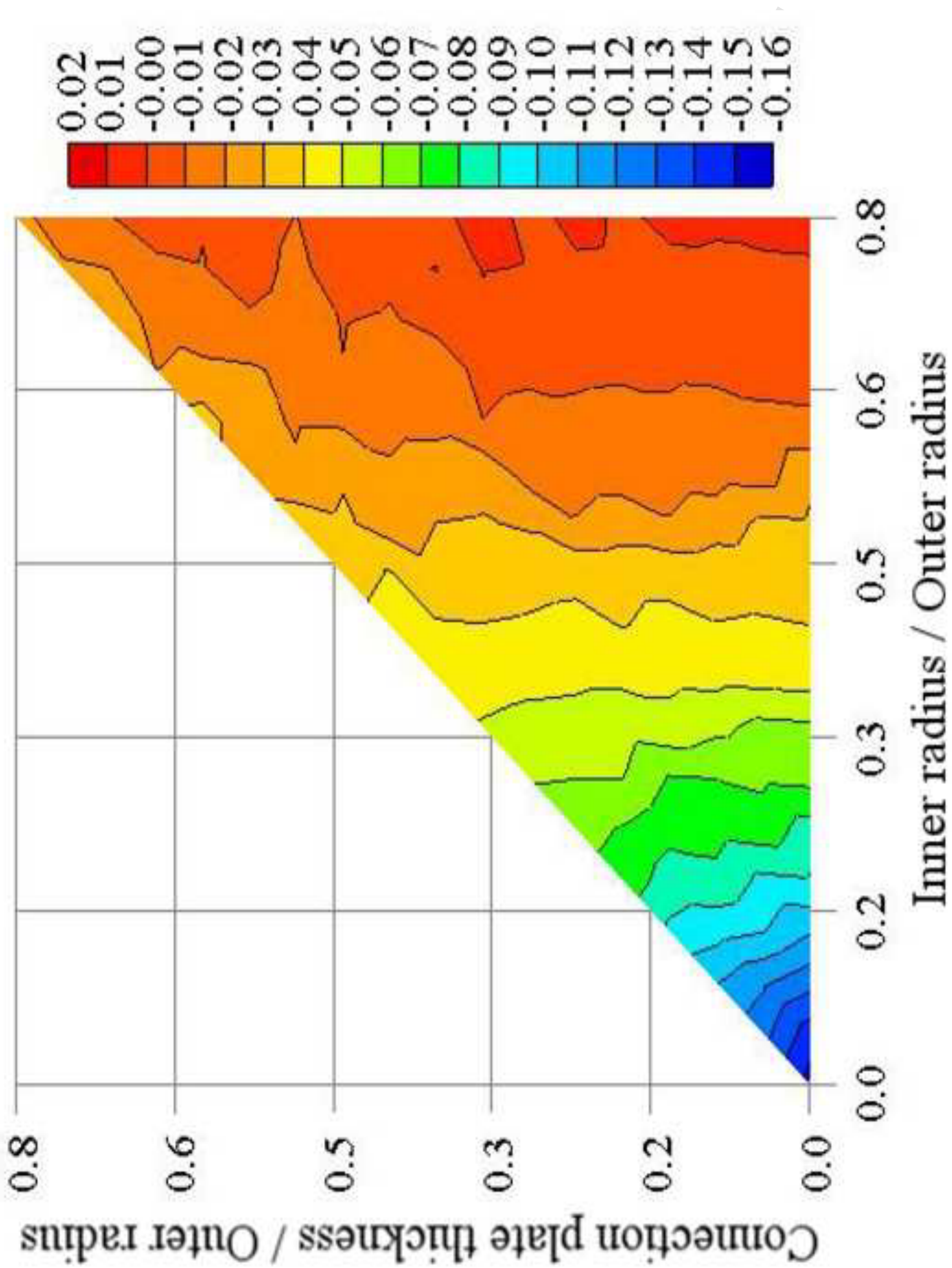
0.02
0.01
-0.00
-0.01
-0.02
-0.03
-0.04
-0.05
-0.06
-0.07
-0.08
-0.09
-0.10
-0.11
-0.12
-0.13
-0.14
-0.15
-0.16
0.0
0.2
0.3
0.5
0.6
0.8
Inner radius / Outer radius
Connection plate thickness / Outer radius

Figure

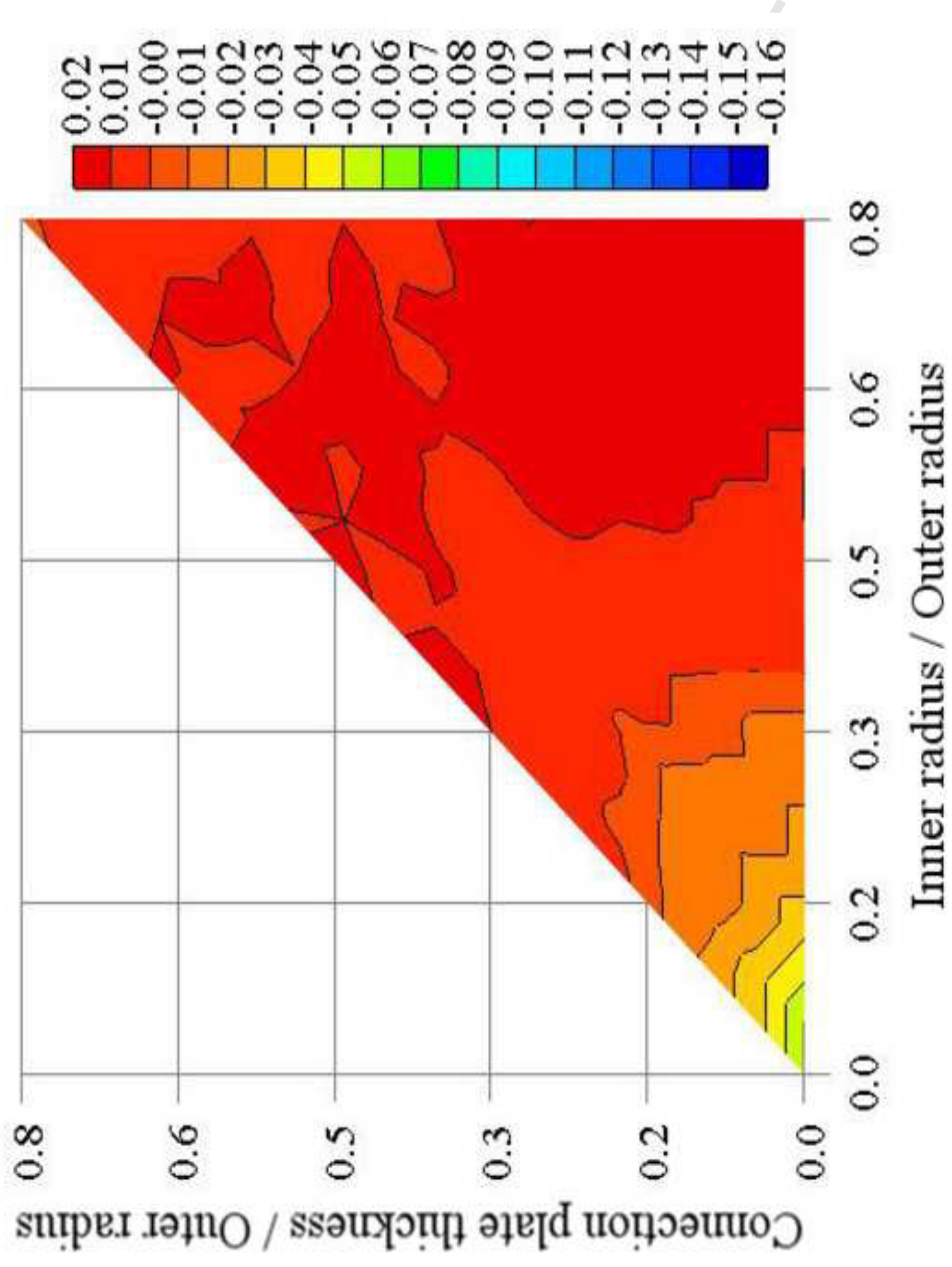
0.02
0.01
-0.00
-0.01
-0.02
-0.03
-0.04
-0.05
-0.06
-0.07
-0.08
-0.09
-0.10
-0.11
-0.12
-0.13
-0.14
-0.15
-0.16
0.0
0.2
0.3
0.5
0.6
0.8
Inner radius / Outer radius
Connection plate thickness / Outer radius

Figure

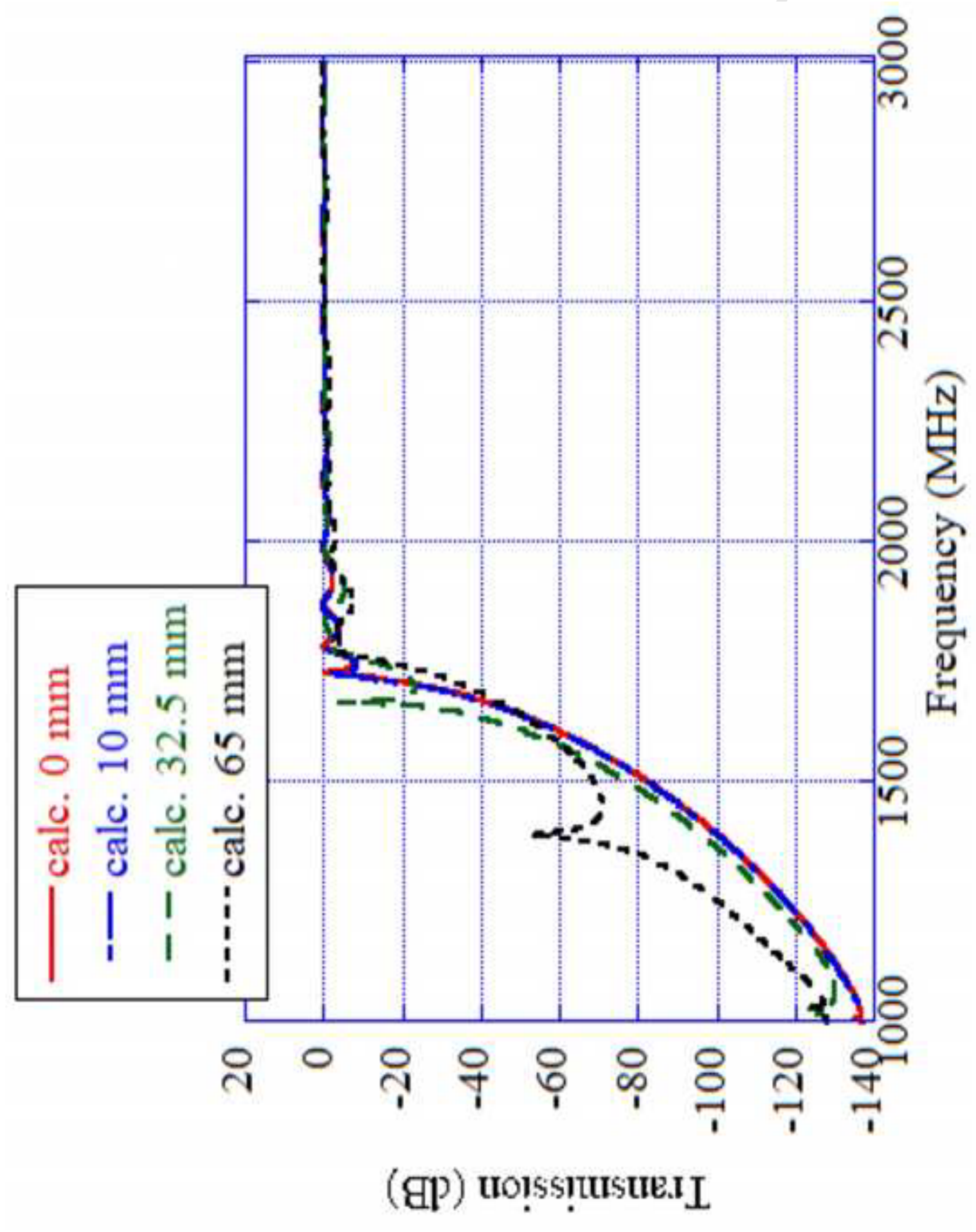

calc. 0 mm
calc. 10 mm
calc. 32.5 mm
calc. 65 mm
Transmission (dB)
Frequency (MHz)
20
0
-20
-40
-60
-80
-100
-120
-140
1000
1500
2000
2500
3000

Figure

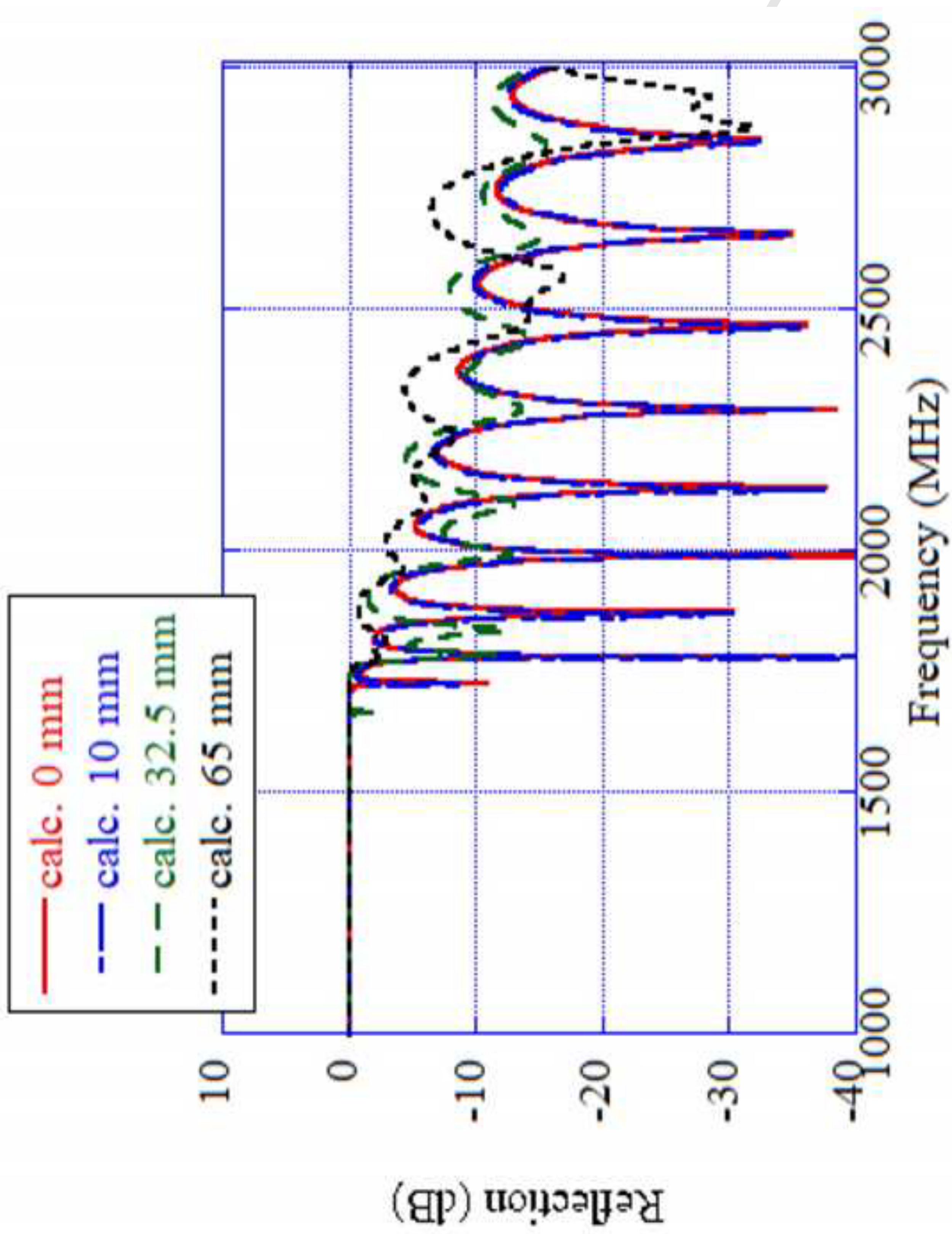

calc. 0 mm
calc. 10 mm
calc. 32.5 mm
calc. 65 mm
Reflection (dB)
Frequency (MHz)
10
0
-10
-20
-30
-40
1000
1500
2000
2500
3000

Figure

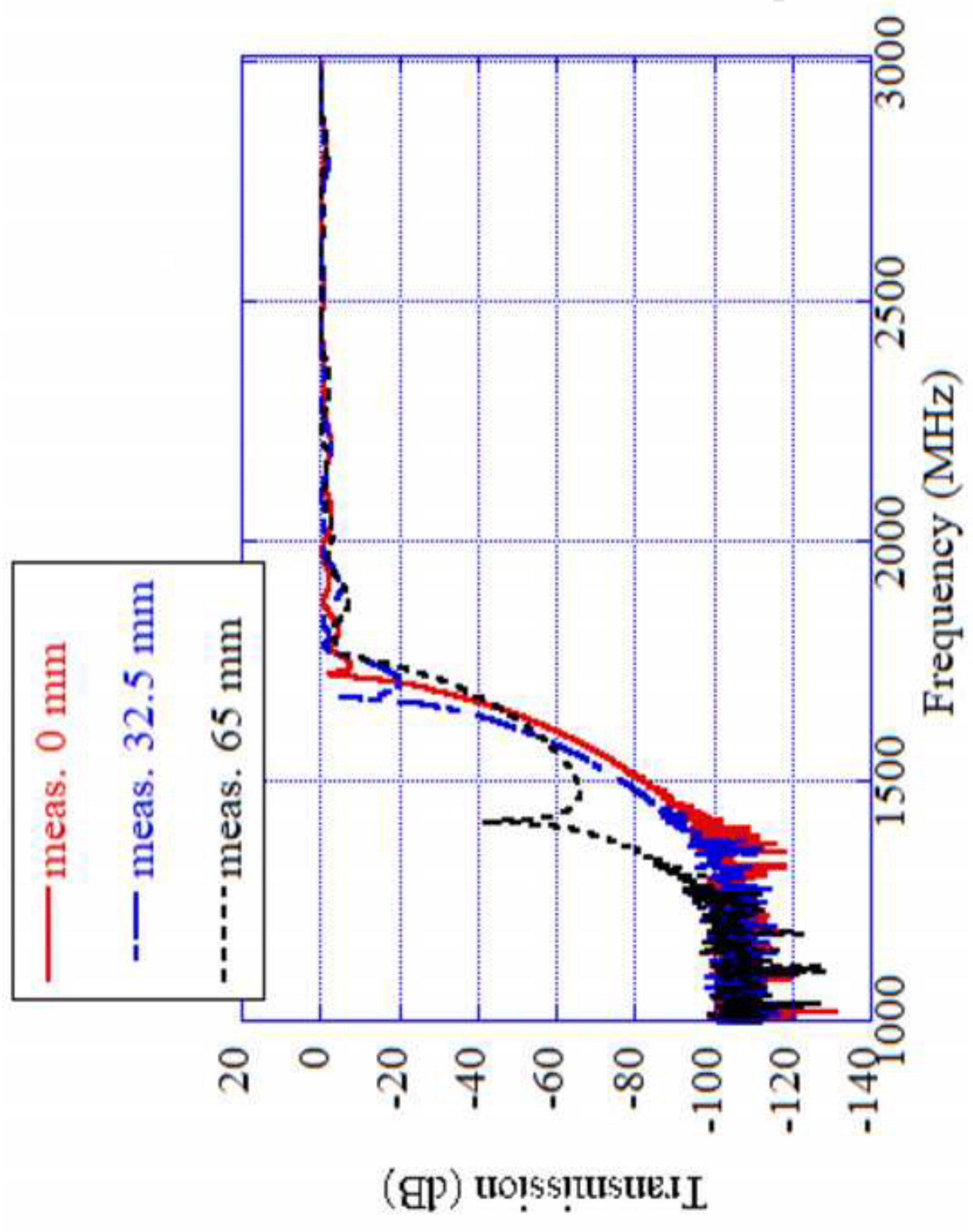

meas. 0 mm
meas. 32.5 mm
meas. 65 mm
Transmission (dB)
Frequency (MHz)
20
0
-20
-40
-60
-80
-100
-120
-140
1000
1500
2000
2500
3000

Figure

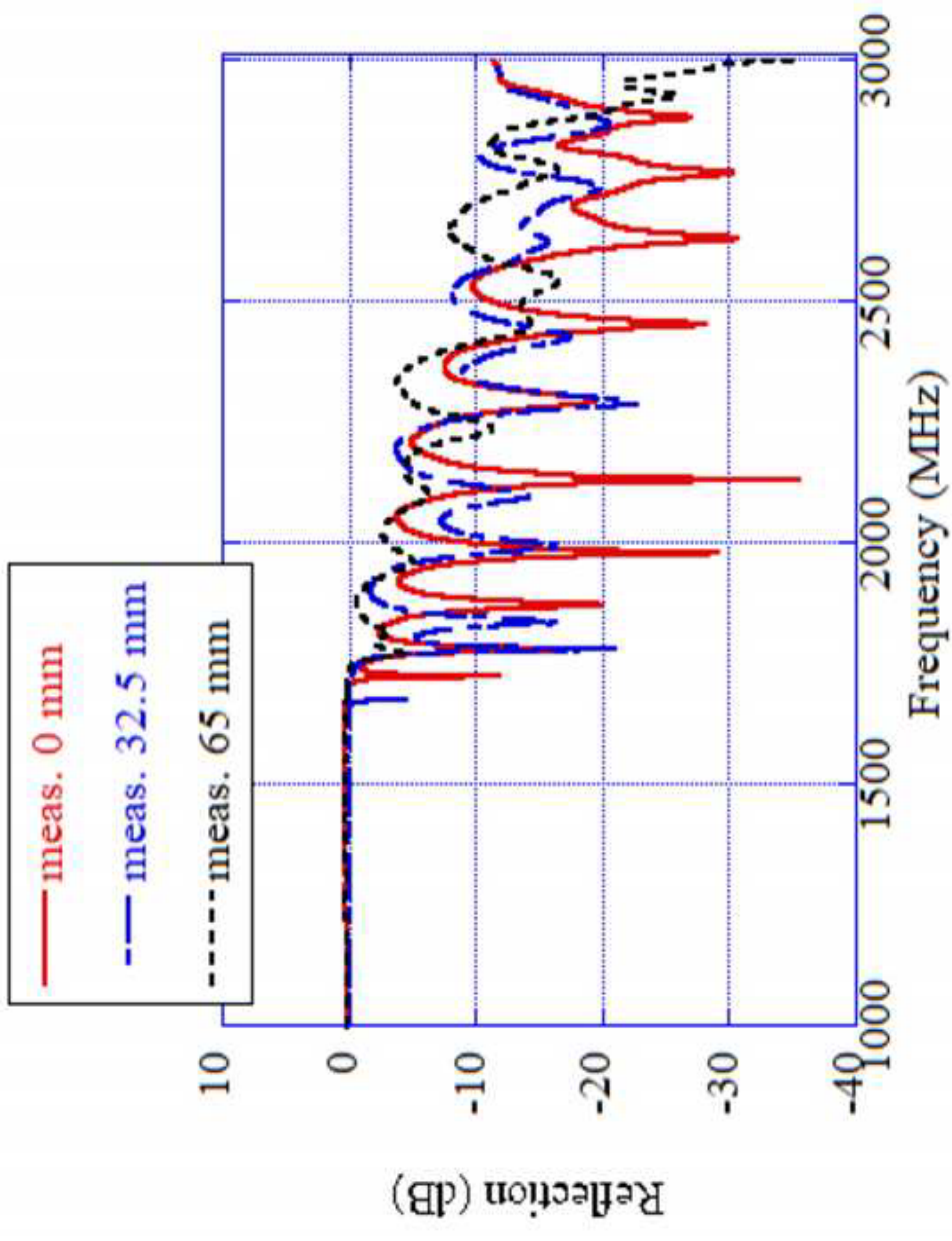

meas. 0 mm
meas. 32.5 mm
meas. 65 mm
10
0
-10
-20
-30
-40
1000
1500
2000
2500
3000
Frequency (MHz)
Reflection (dB)

Figure

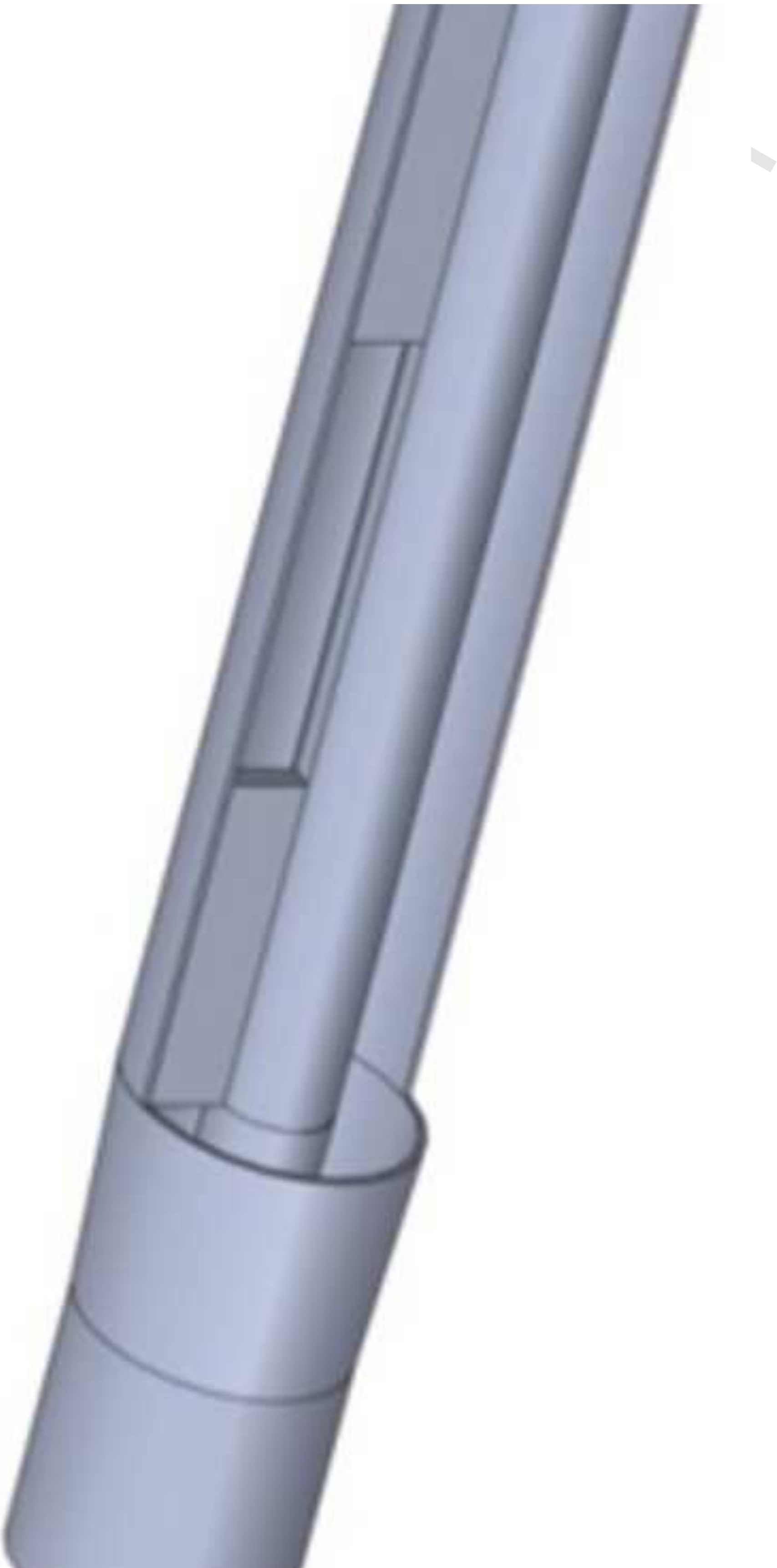

Figure

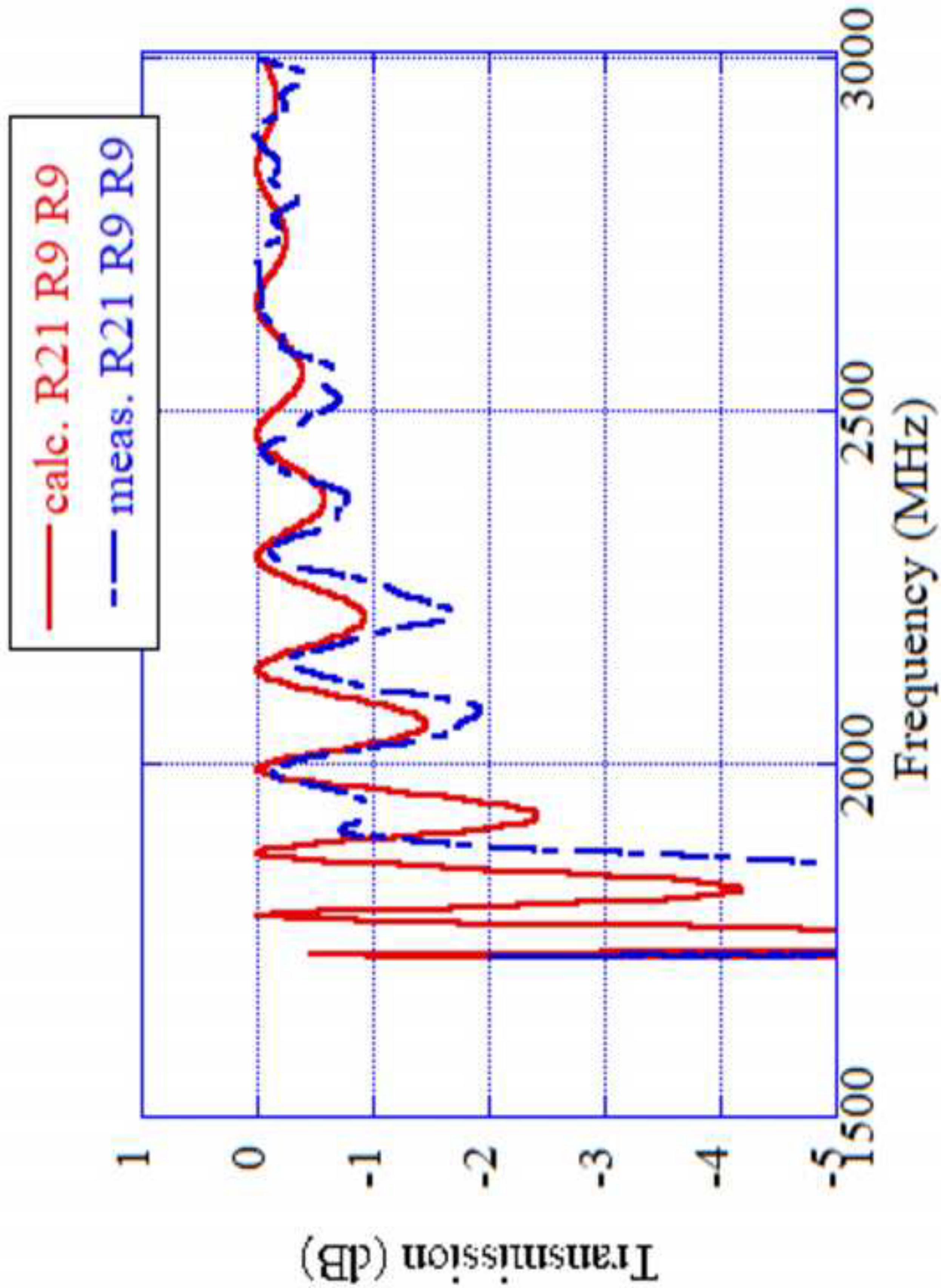

calc. R21 R9 R9
meas. R21 R9 R9
Transmission (dB)
Frequency (MHz)
1
0
-1
-2
-3
-4
-5
1500
2000
2500
3000

Figure

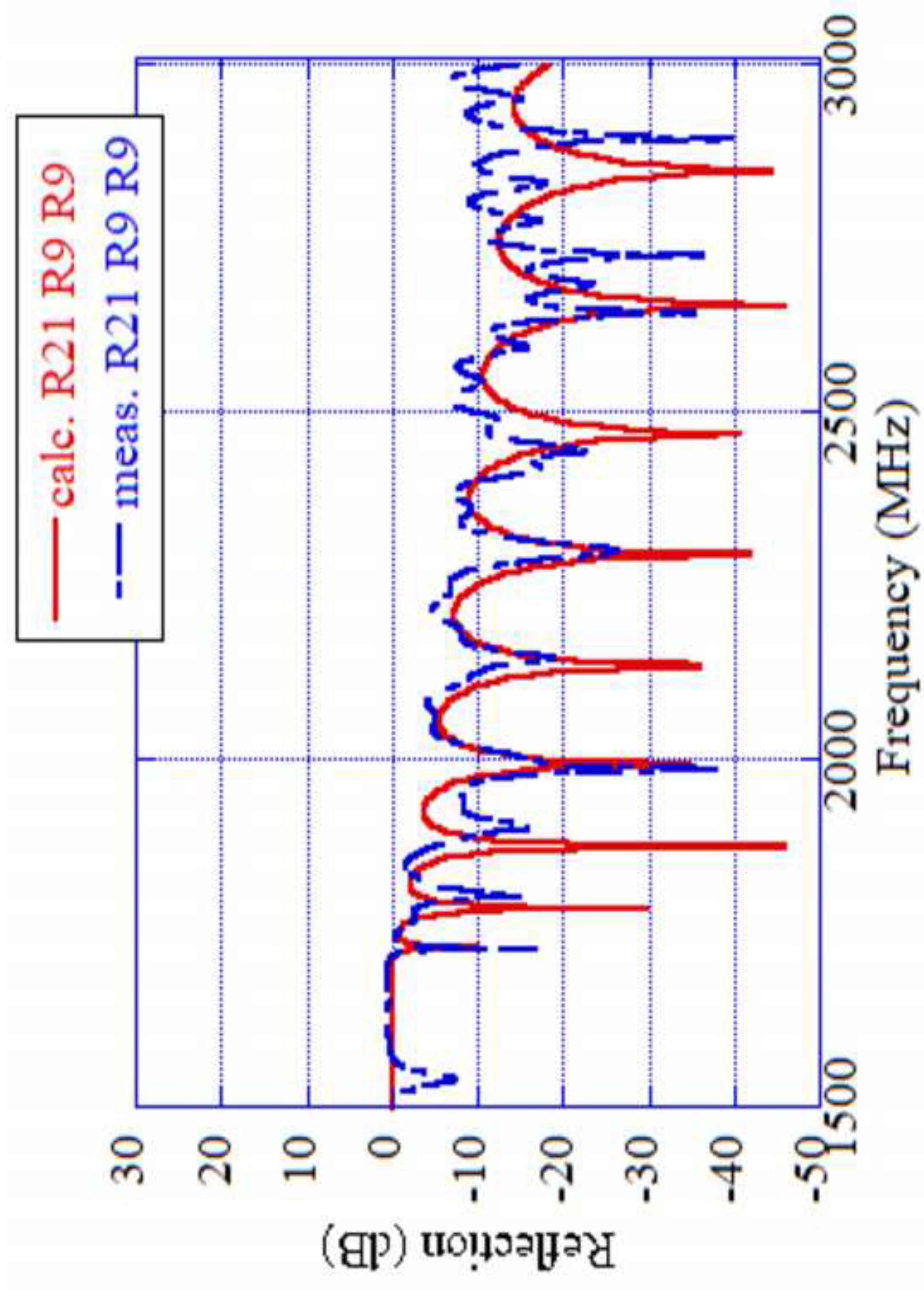
calc. R21 R9 R9
meas. R21 R9 R9
Reflection (dB)
Frequency (MHz)
30
20
10
0
-10
-20
-30
-40
-50
1500
2000
2500
3000

Figure

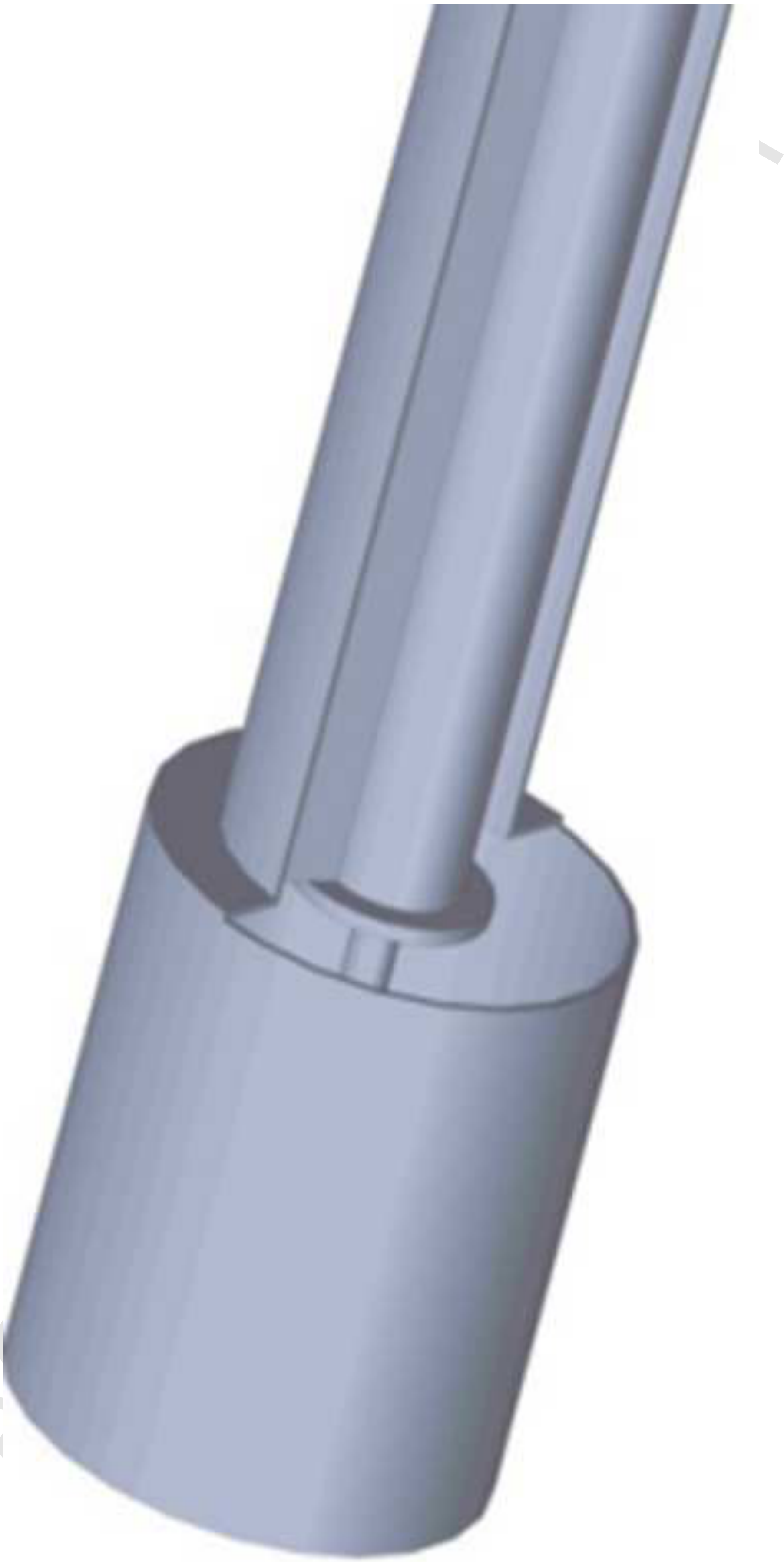

Figure

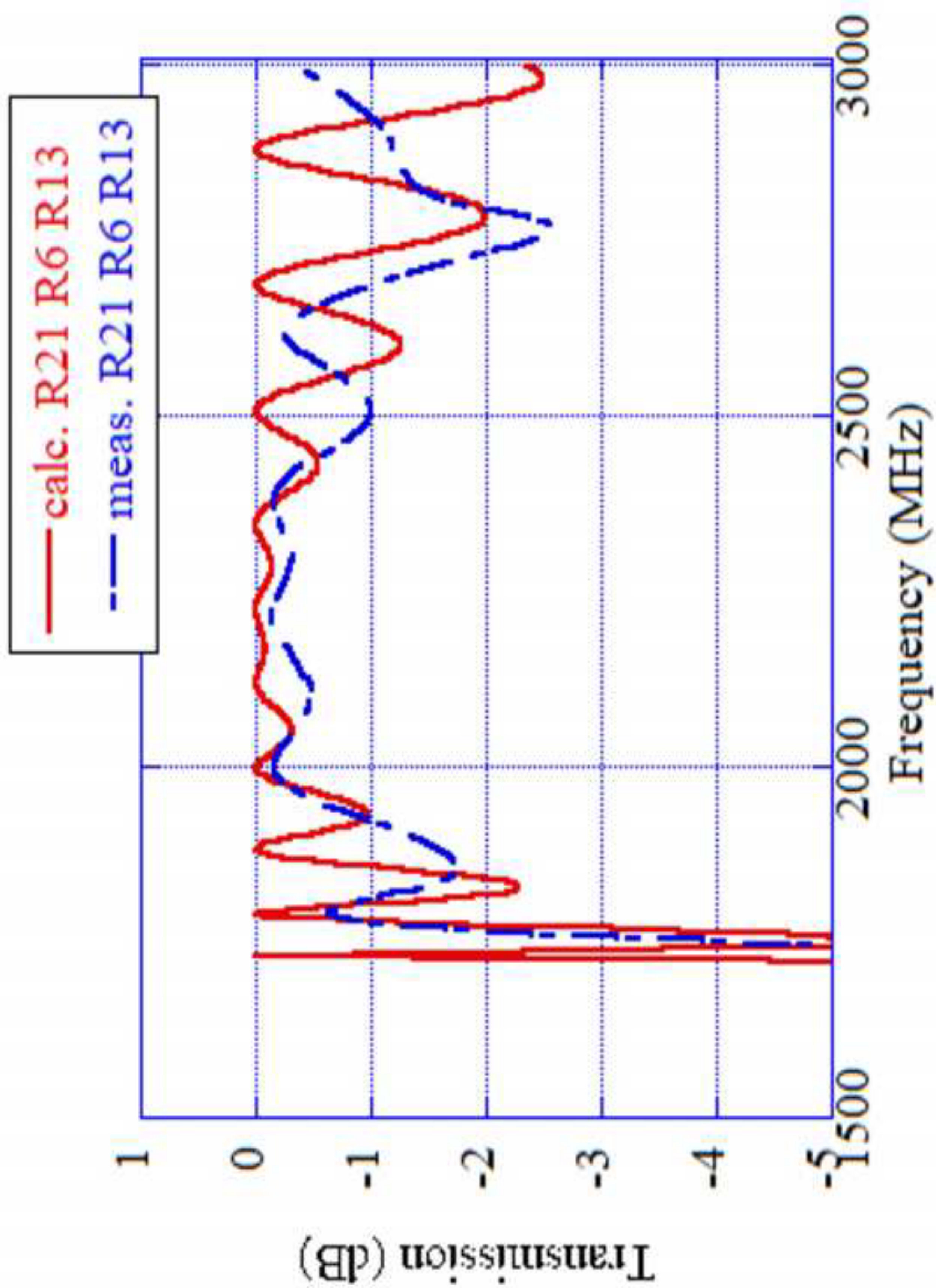
calc. R21 R6 R13
meas. R21 R6 R13
Transmission (dB)
Frequency (MHz)
1
0
-1
-2
-3
-4
-5
1500
2000
2500
3000

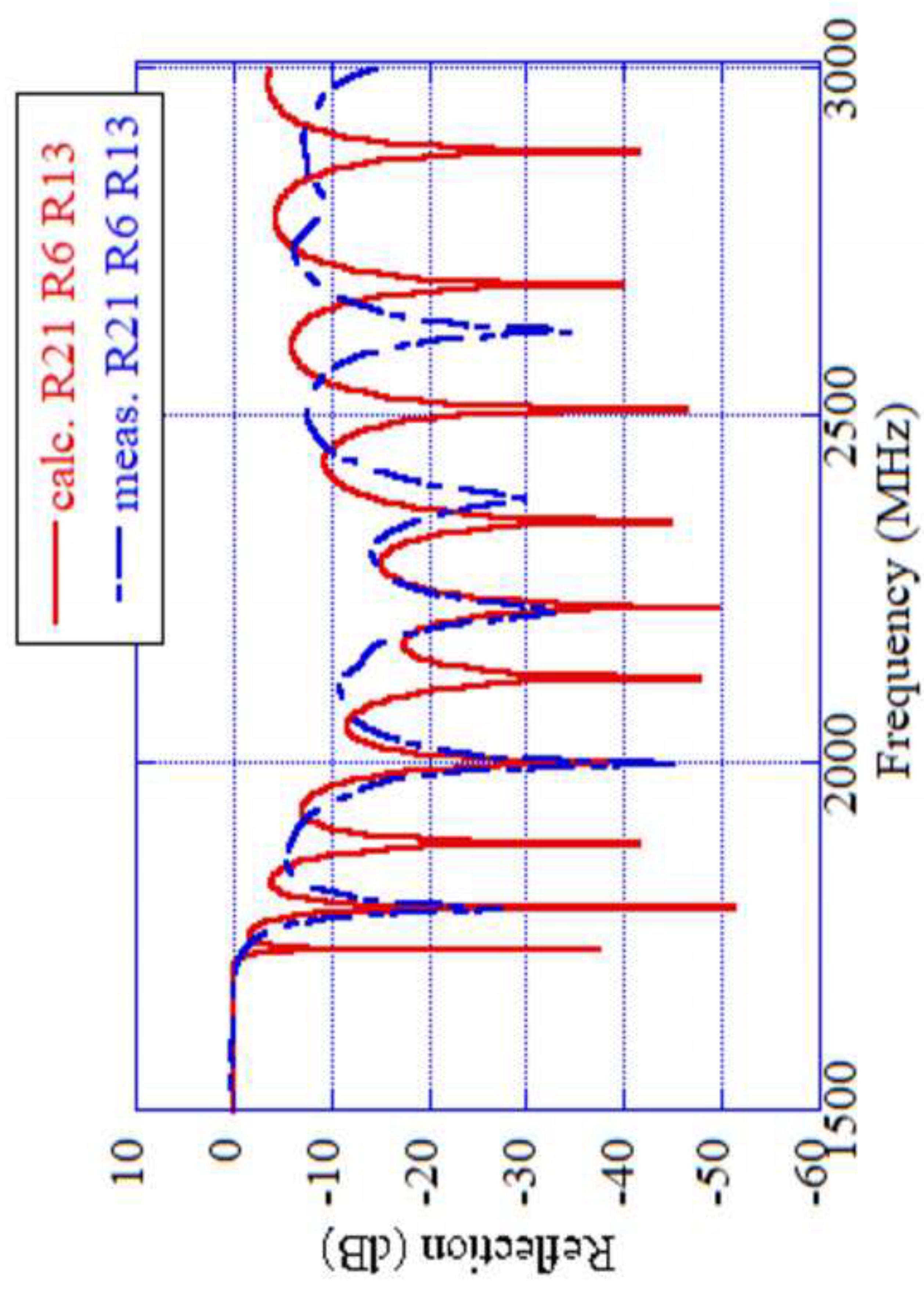
calc. R21 R6 R13
meas. R21 R6 R13
Reflection (dB)
Frequency (MHz)
10
0
-10
-20
-30
-40
-50
-60
1500
2000
2500
3000

Figure

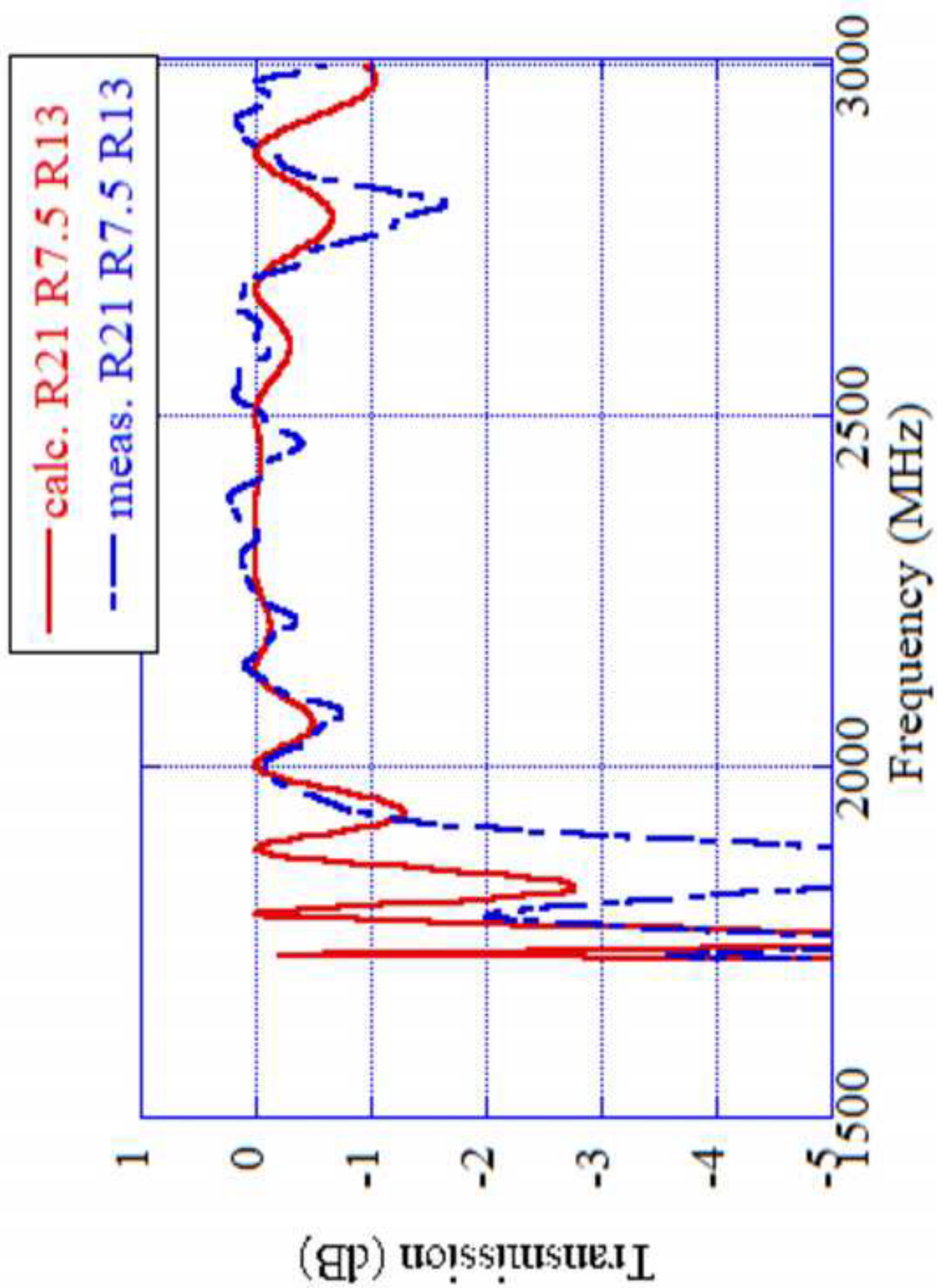

calc. R21 R7.5 R13
meas. R21 R7.5 R13
Transmission (dB)
Frequency (MHz)
1
0
-1
-2
-3
-4
-5
1500
2000
2500
3000

Figure

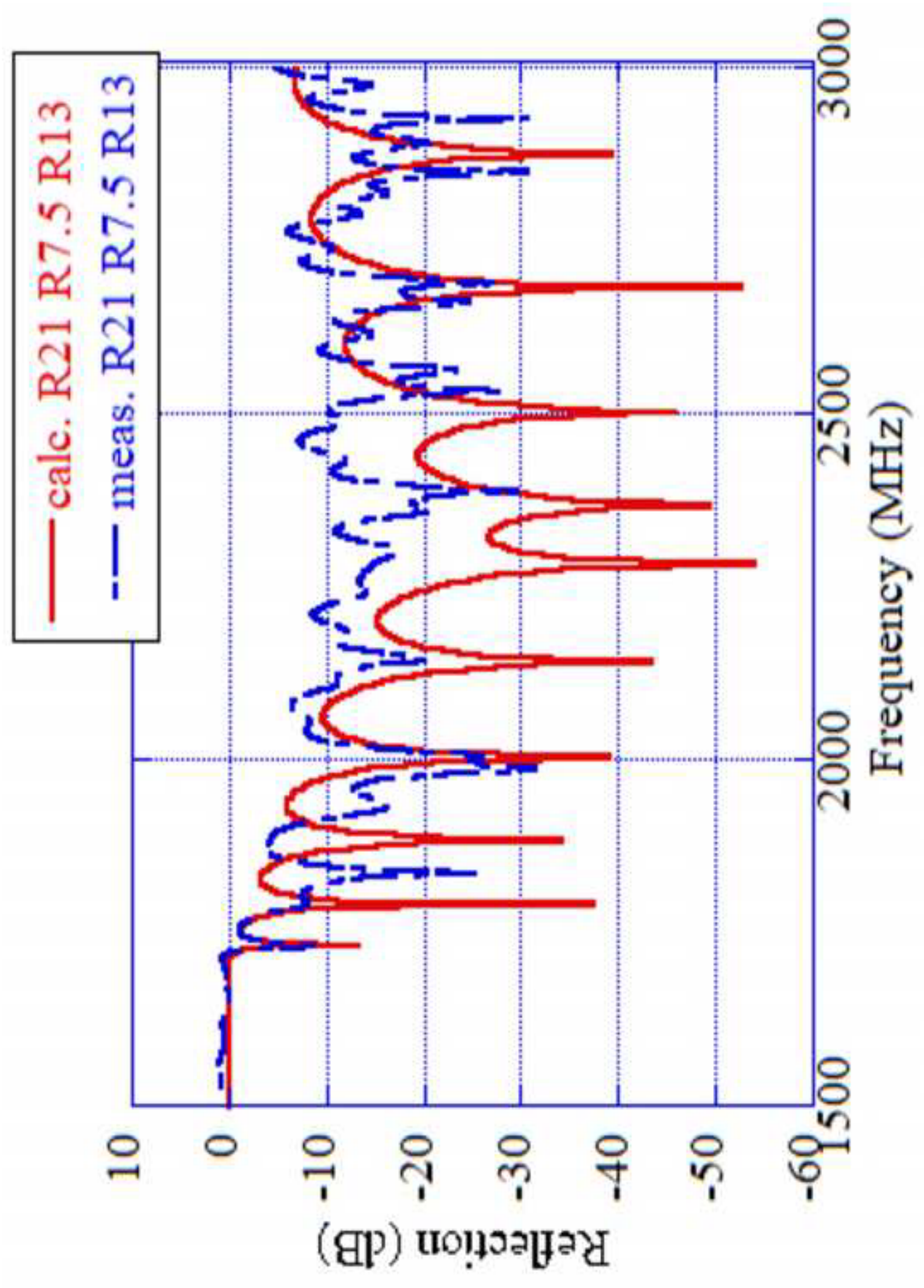
calc. R21 R7.5 R13
meas. R21 R7.5 R13
Reflection (dB)
10
0
-10
-20
-30
-40
-50
-60
1500
2000
2500
3000
Frequency (MHz)

Figure

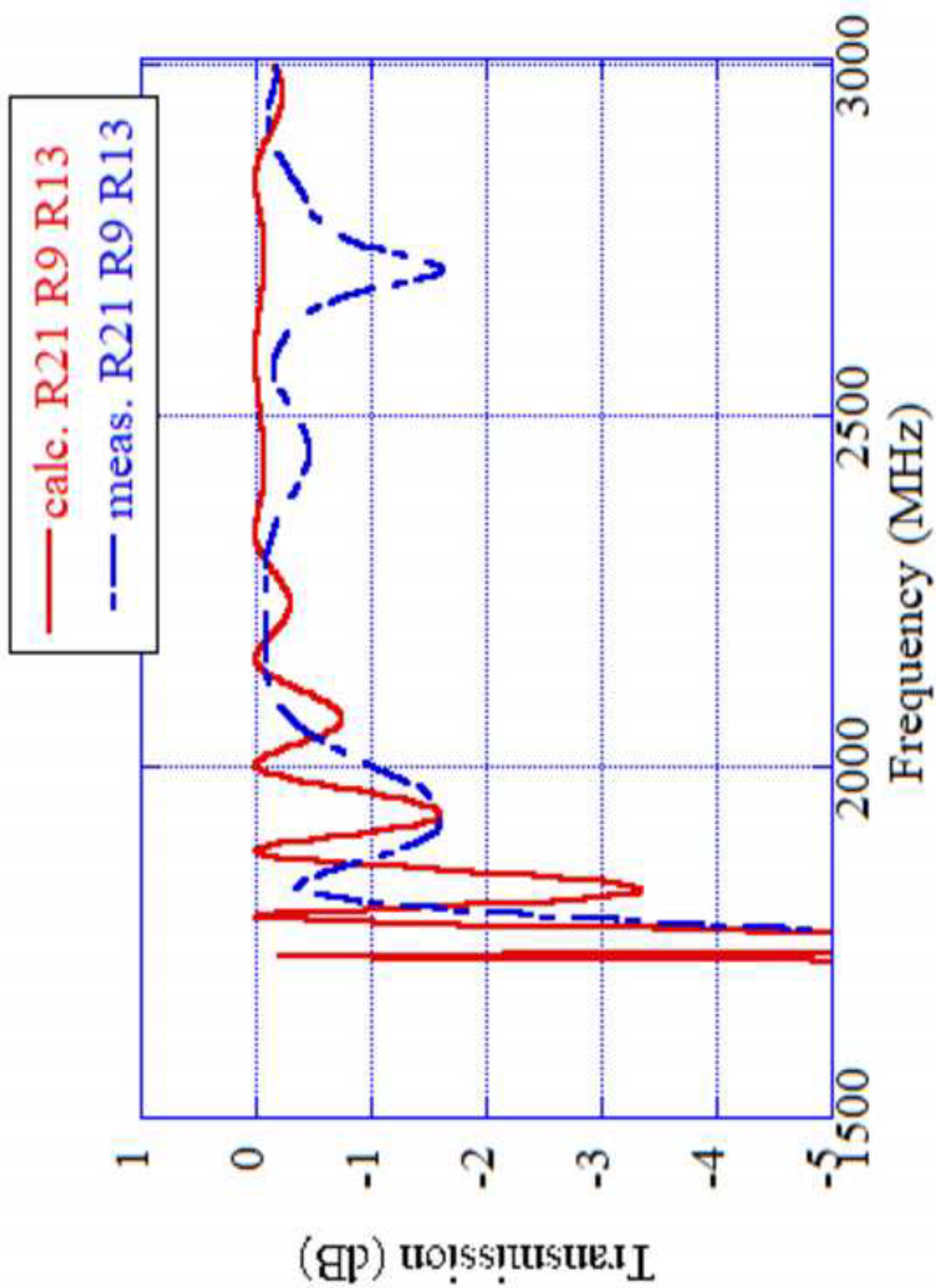

calc. R21 R9 R13
meas. R21 R9 R13
Transmission (dB)
Frequency (MHz)
1
0
-1
-2
-3
-4
-5
1500
2000
2500
3000

Figure

Figure

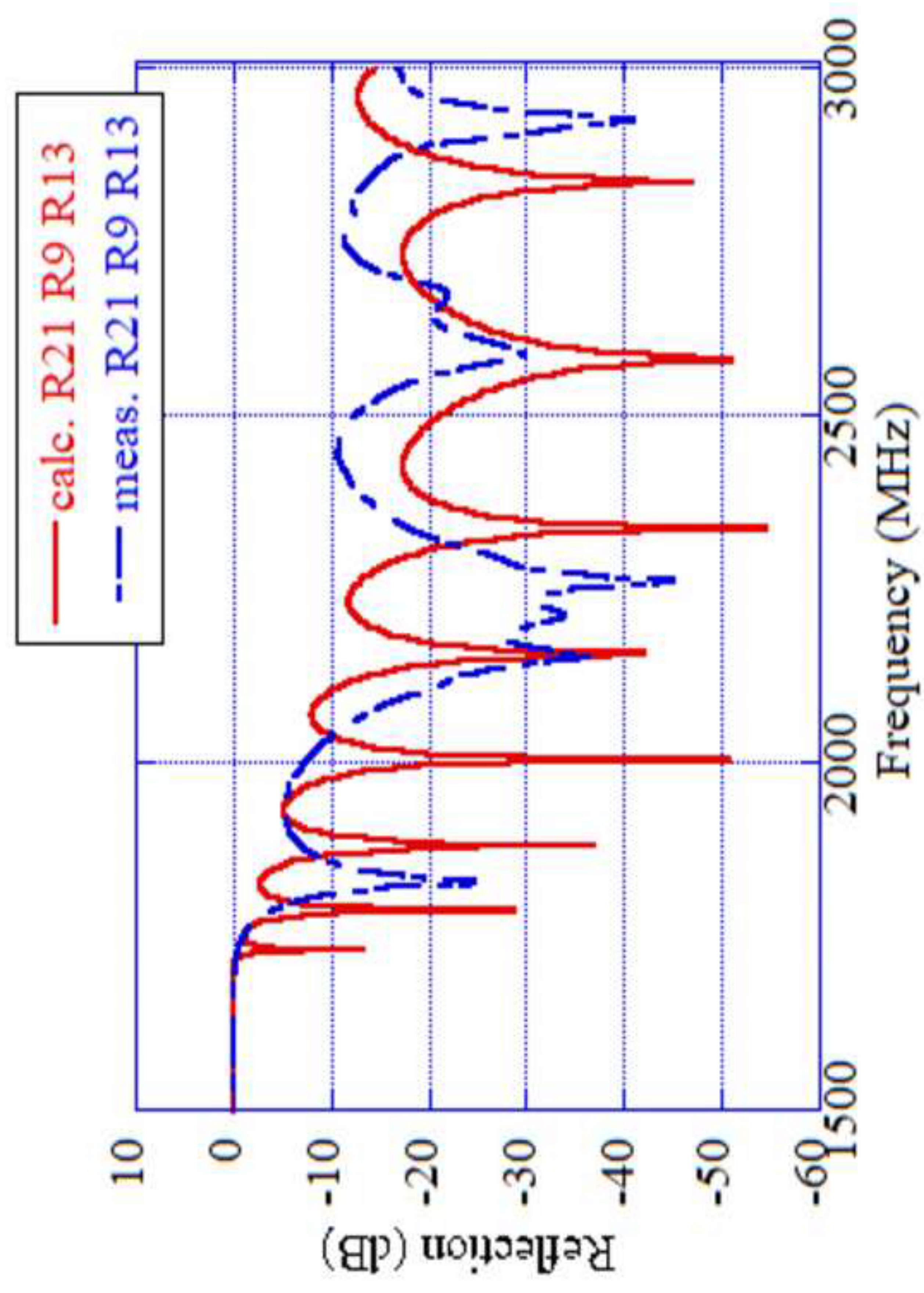

calc. R21 R9 R13
meas. R21 R9 R13
Reflection (dB)
10
0
-10
-20
-30
-40
-50
-60
1500
2000
2500
3000
Frequency (MHz)

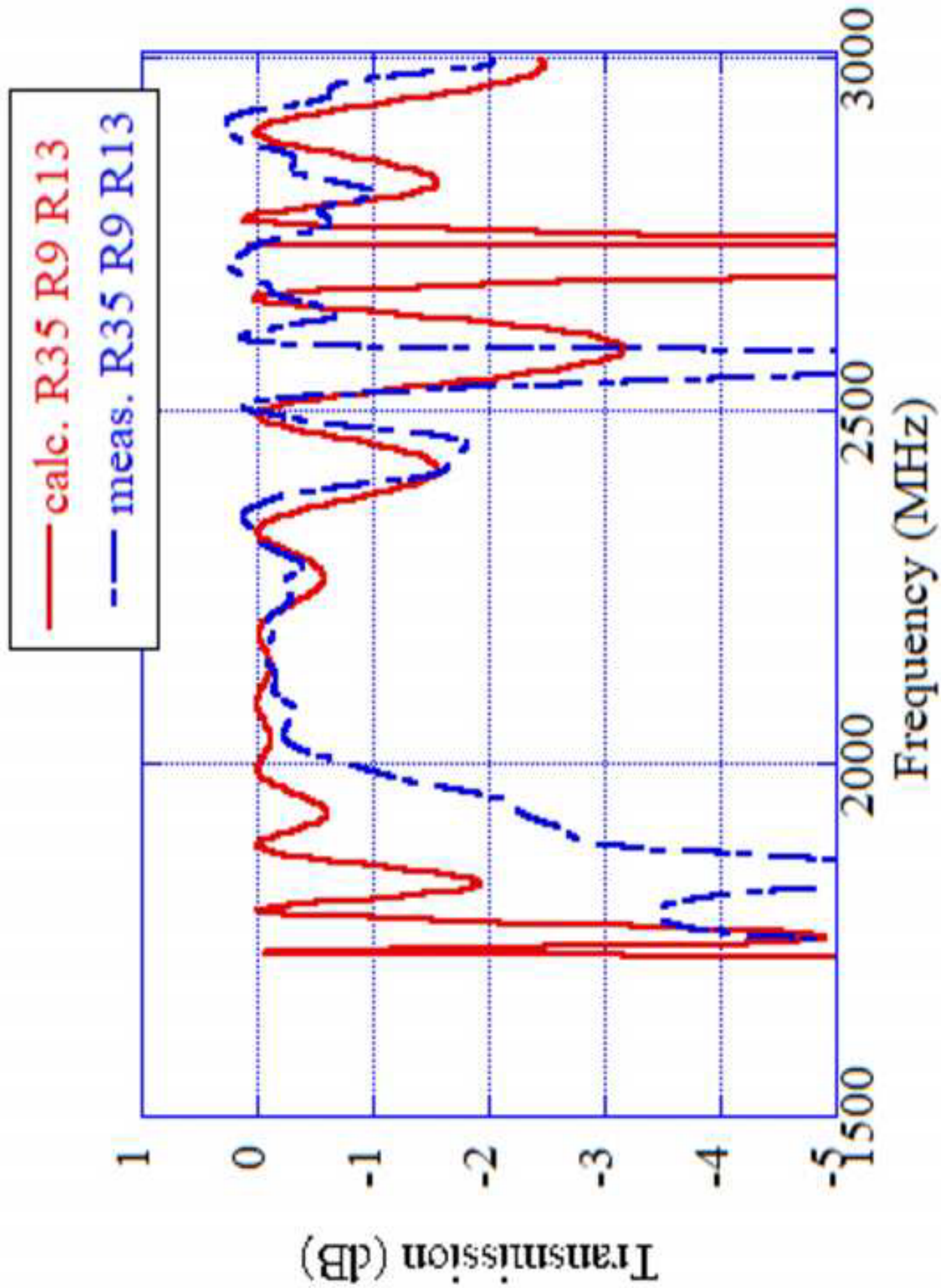

calc. R35 R9 R13
meas. R35 R9 R13
Transmission (dB)
Frequency (MHz)
1
0
-1
-2
-3
-4
-5
1500
2000
2500
3000

Figure

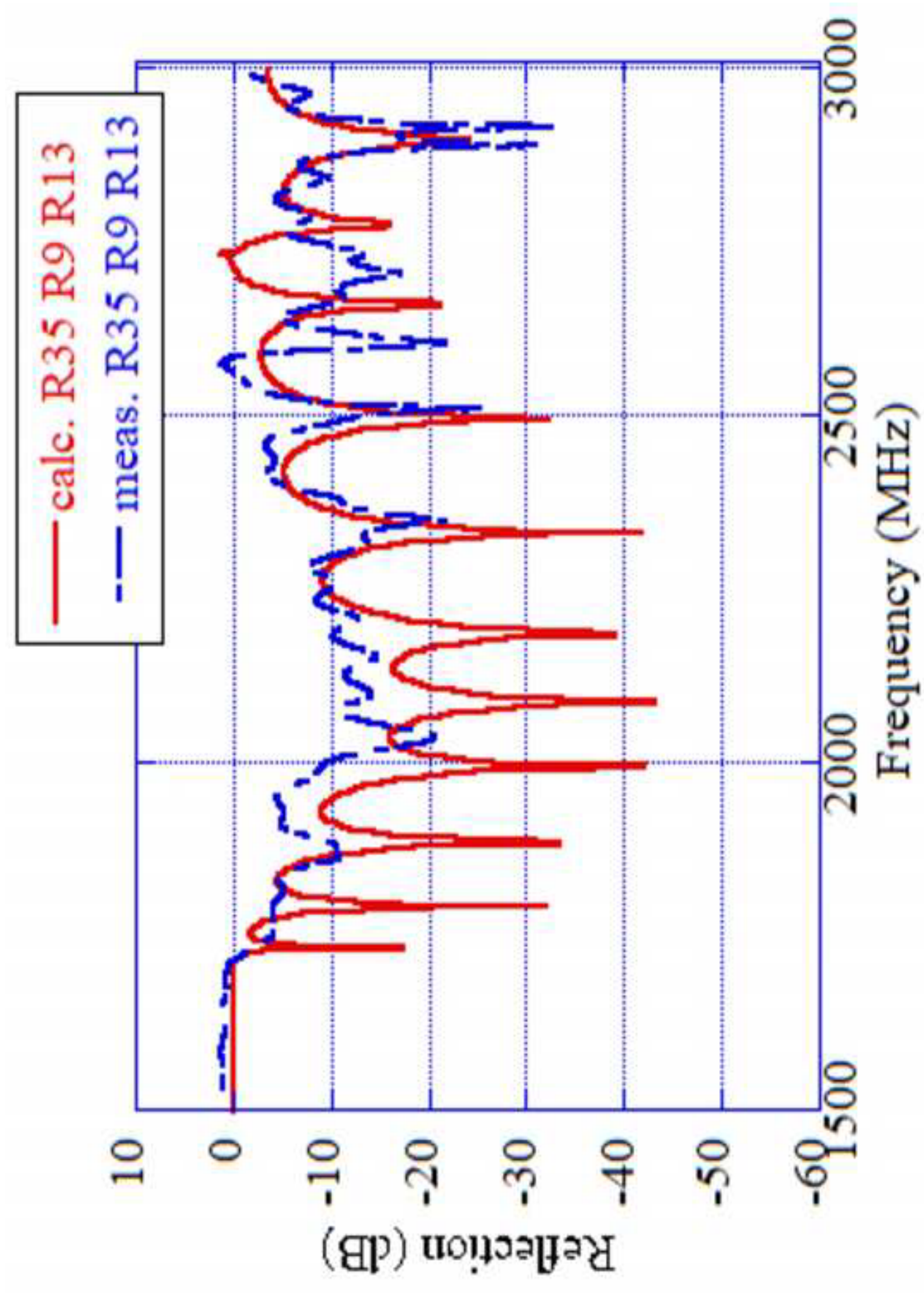
calc. R35 R9 R13
meas. R35 R9 R13
Reflection (dB)
Frequency (MHz)
10
0
-10
-20
-30
-40
-50
-60
1500
2000
2500
3000

Figure

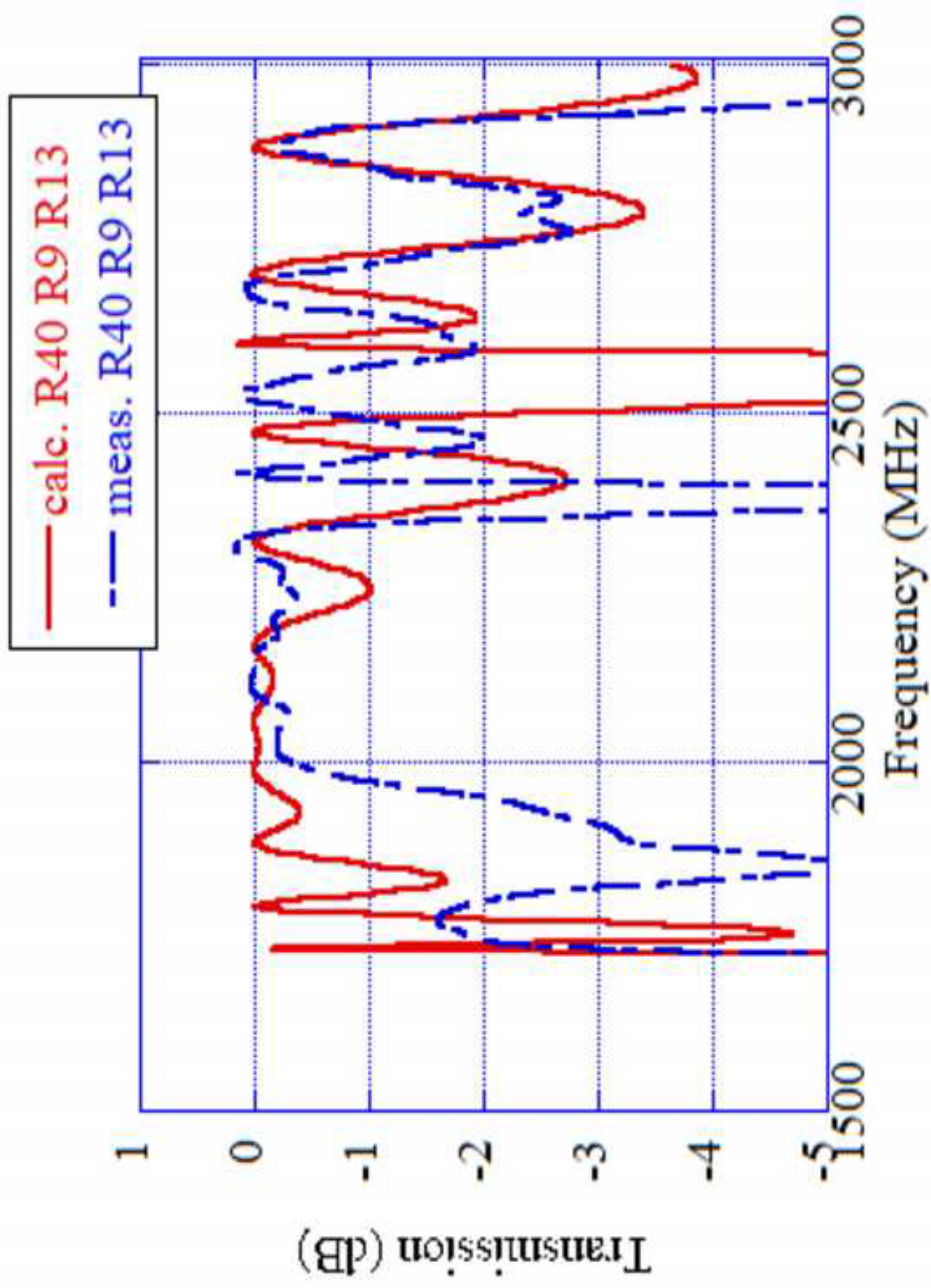

calc. R40 R9 R13
meas. R40 R9 R13
Transmission (dB)
Frequency (MHz)
1
0
-1
-2
-3
-4
-5
1500
2000
2500
3000

Figure

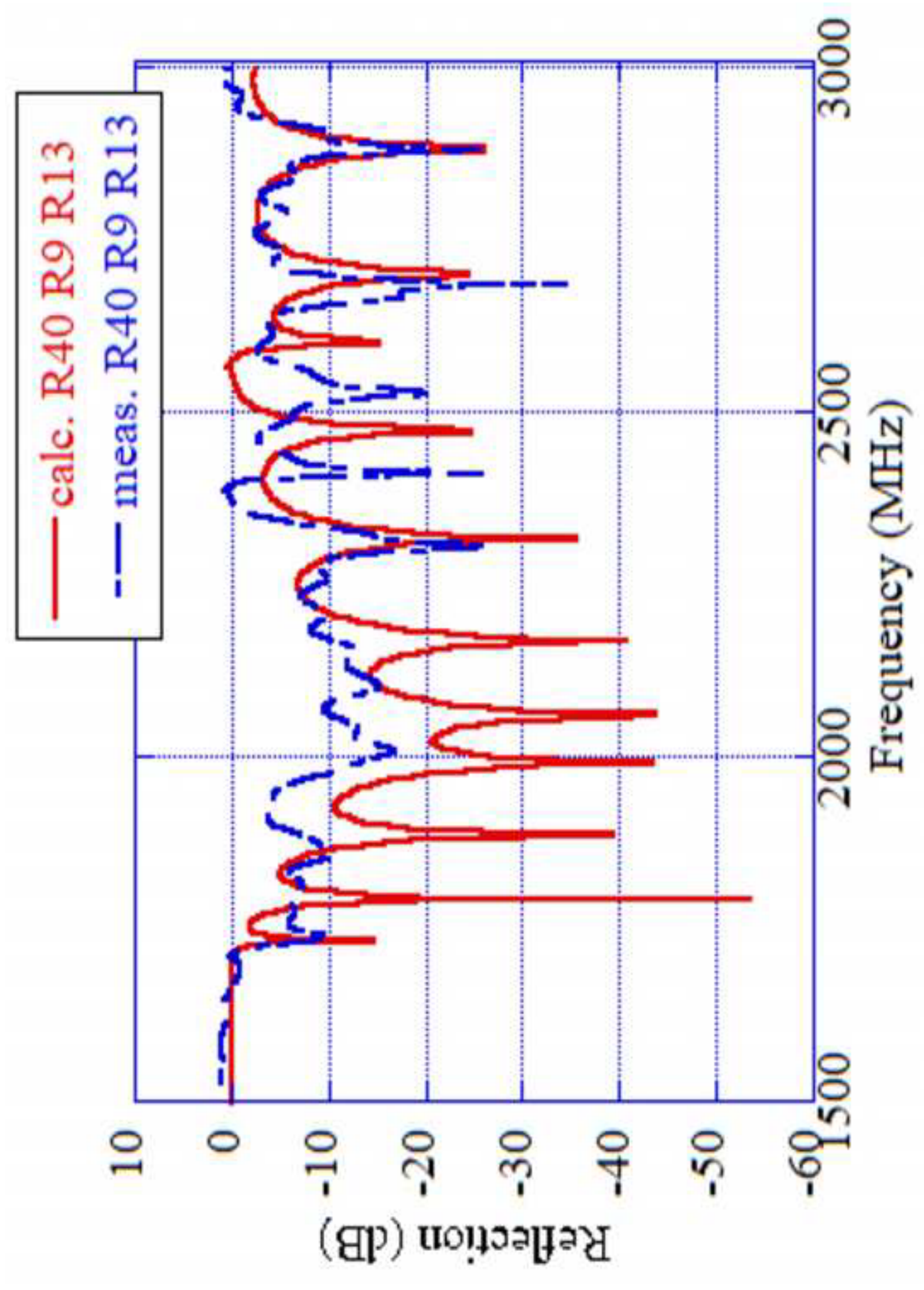

calc. R40 R9 R13
meas. R40 R9 R13
Reflection (dB)
10
0
-10
-20
-30
-40
-50
-60
1500
2000
2500
3000
Frequency (MHz)

Figure

Figure

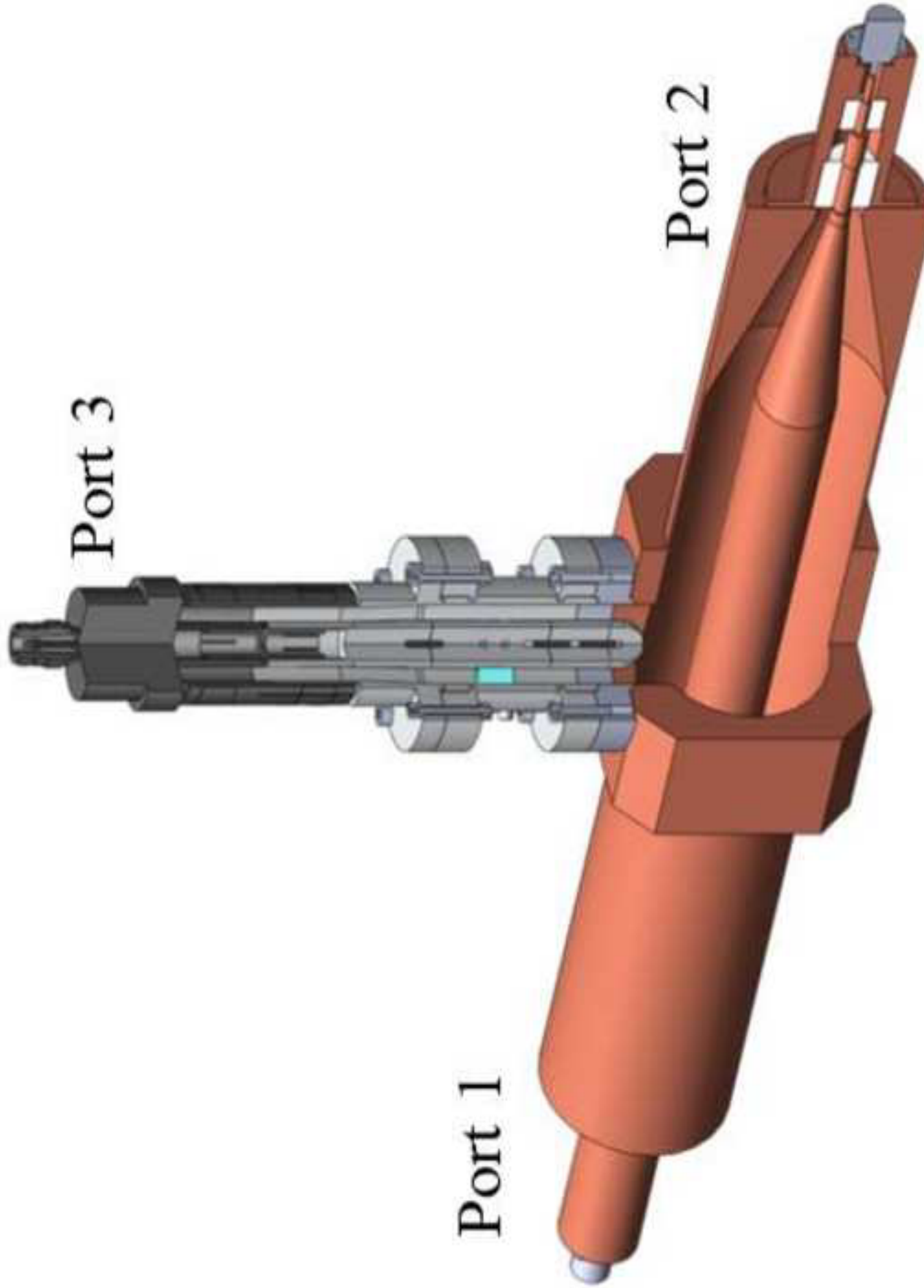

Figure

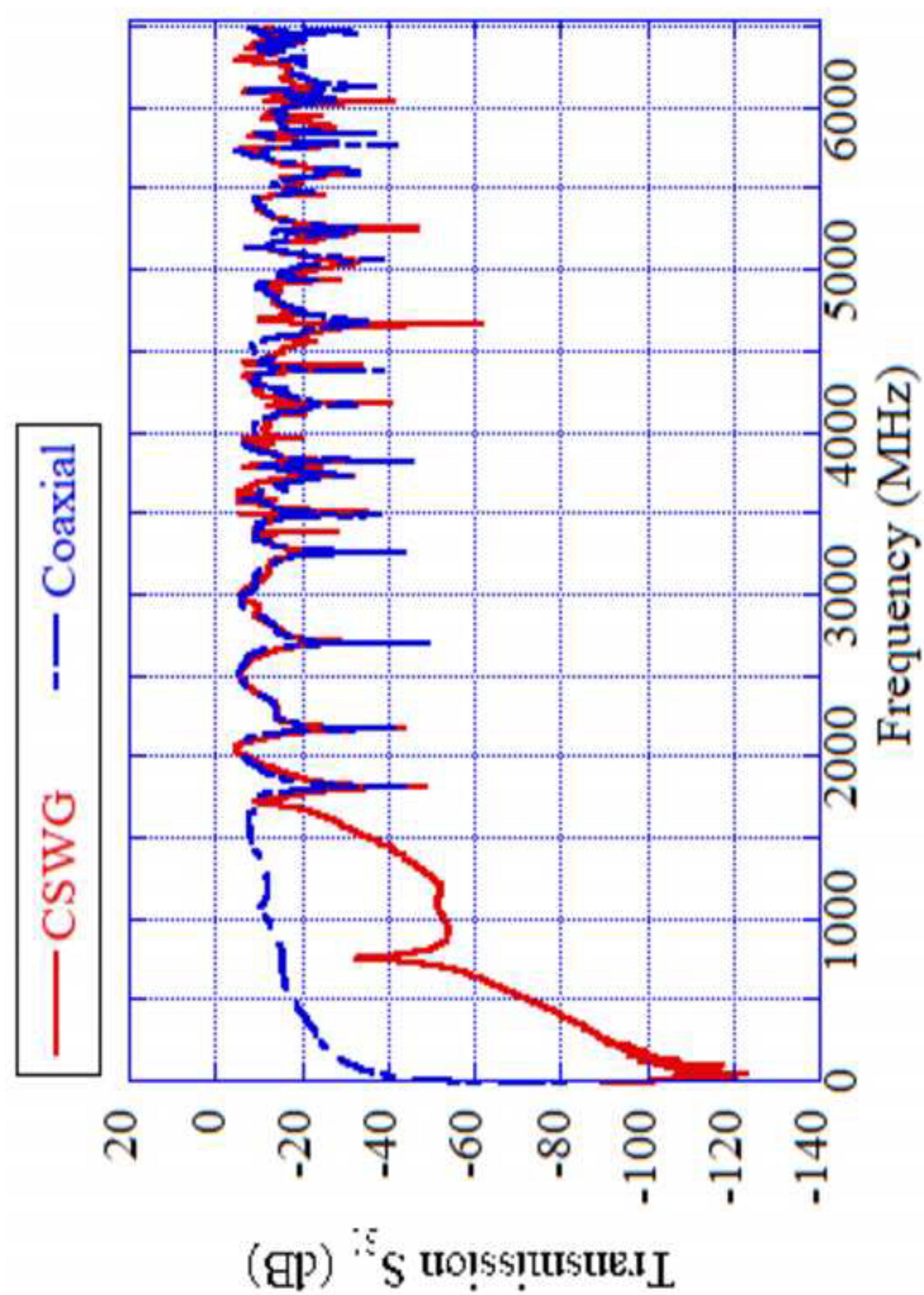
CSWG
Coaxial
Transmission S_{21} (dB)
Frequency (MHz)
20
0
-20
-40
-60
-80
-100
-120
-140
0
1000
2000
3000
4000
5000
6000

Figure

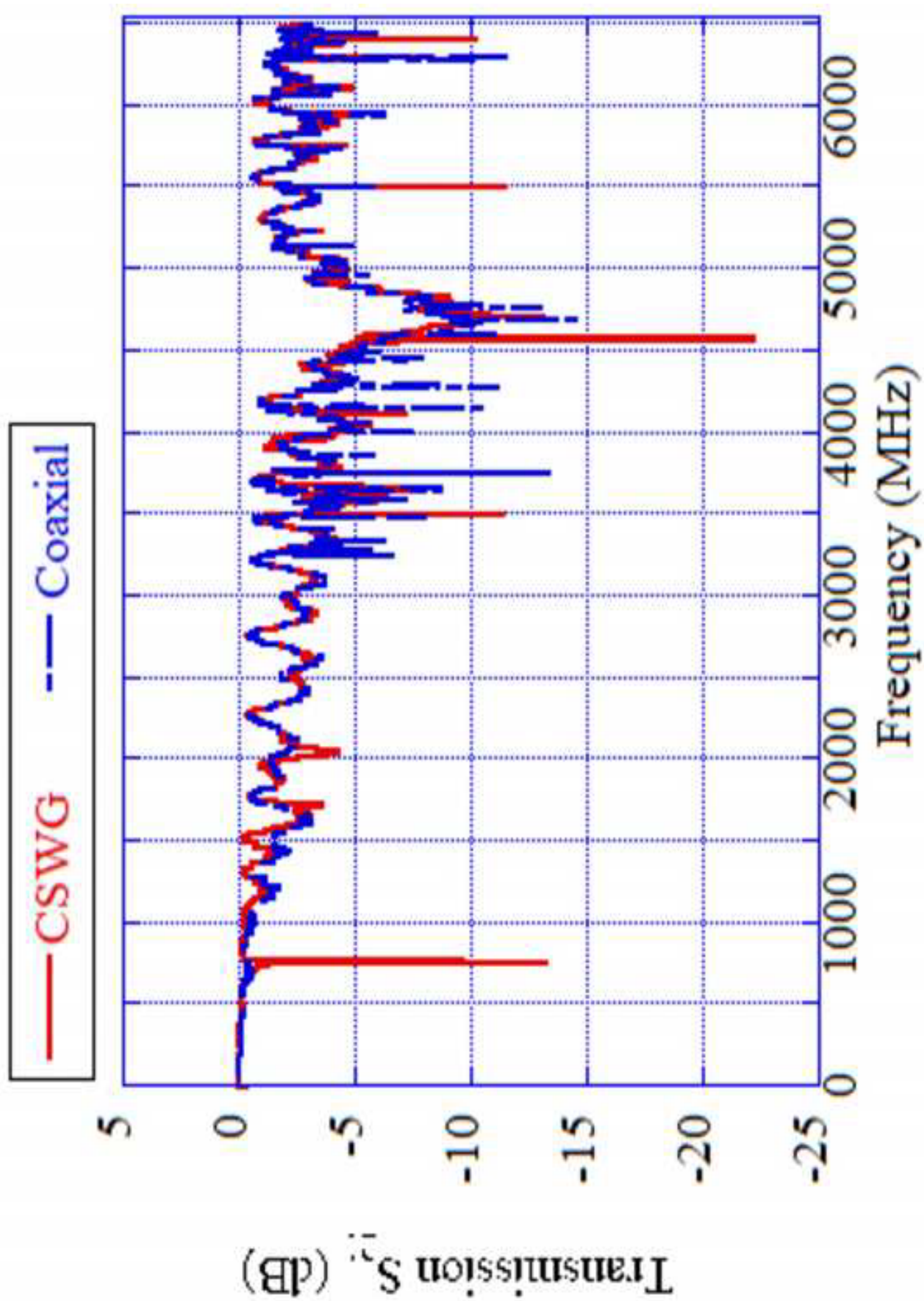
CSWG
Coaxial
5
0
-5
-10
-15
-20
-25
0
1000
2000
3000
4000
5000
6000
Frequency (MHz)
Transmission S_{21} (dB)

Figure

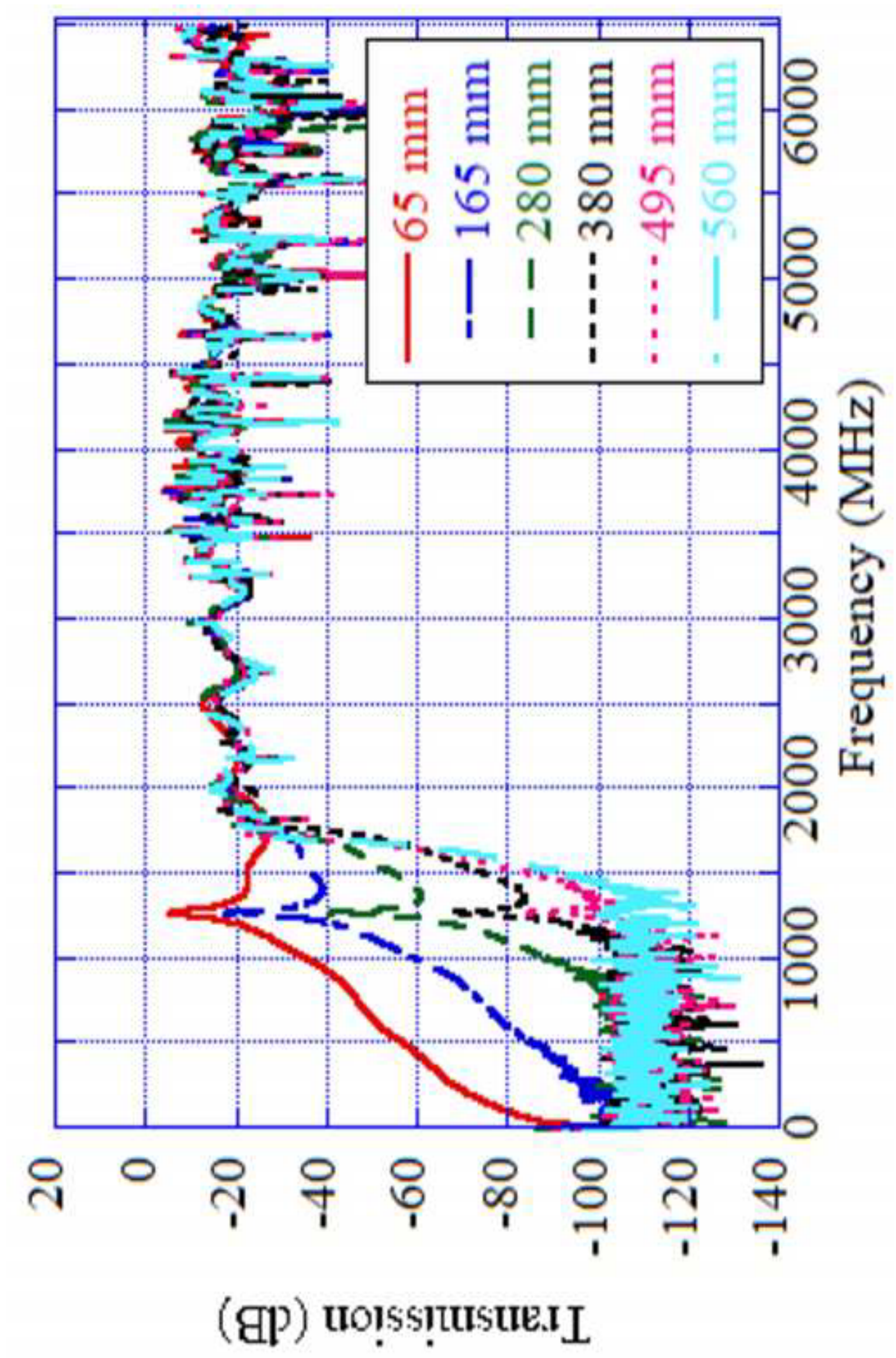

Transmission (dB)
20
0
-20
-40
-60
-80
-100
-120
-140
Frequency (MHz)
0
1000
2000
3000
4000
5000
6000
65 mm
165 mm
280 mm
380 mm
495 mm
560 mm

Figure

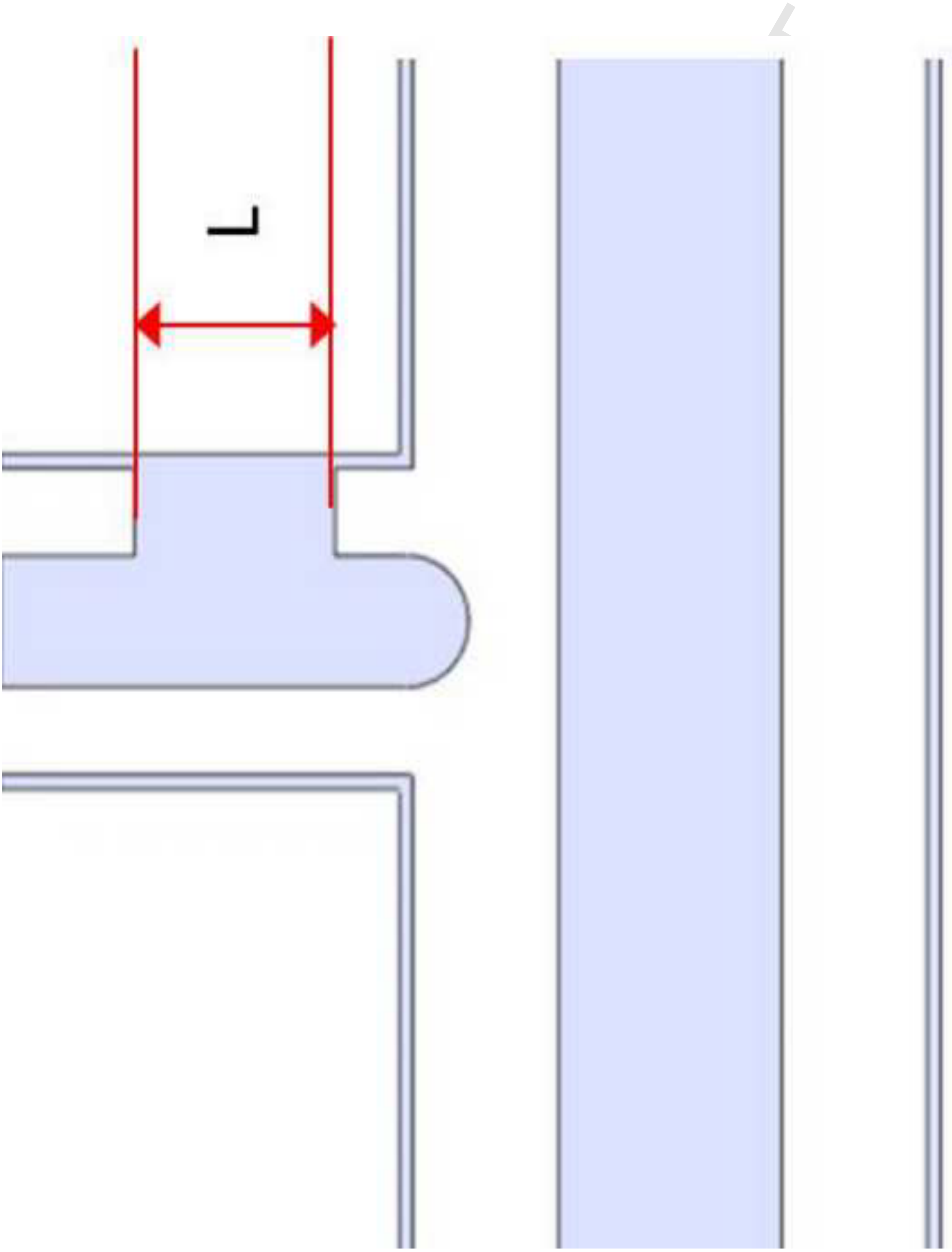

Figure

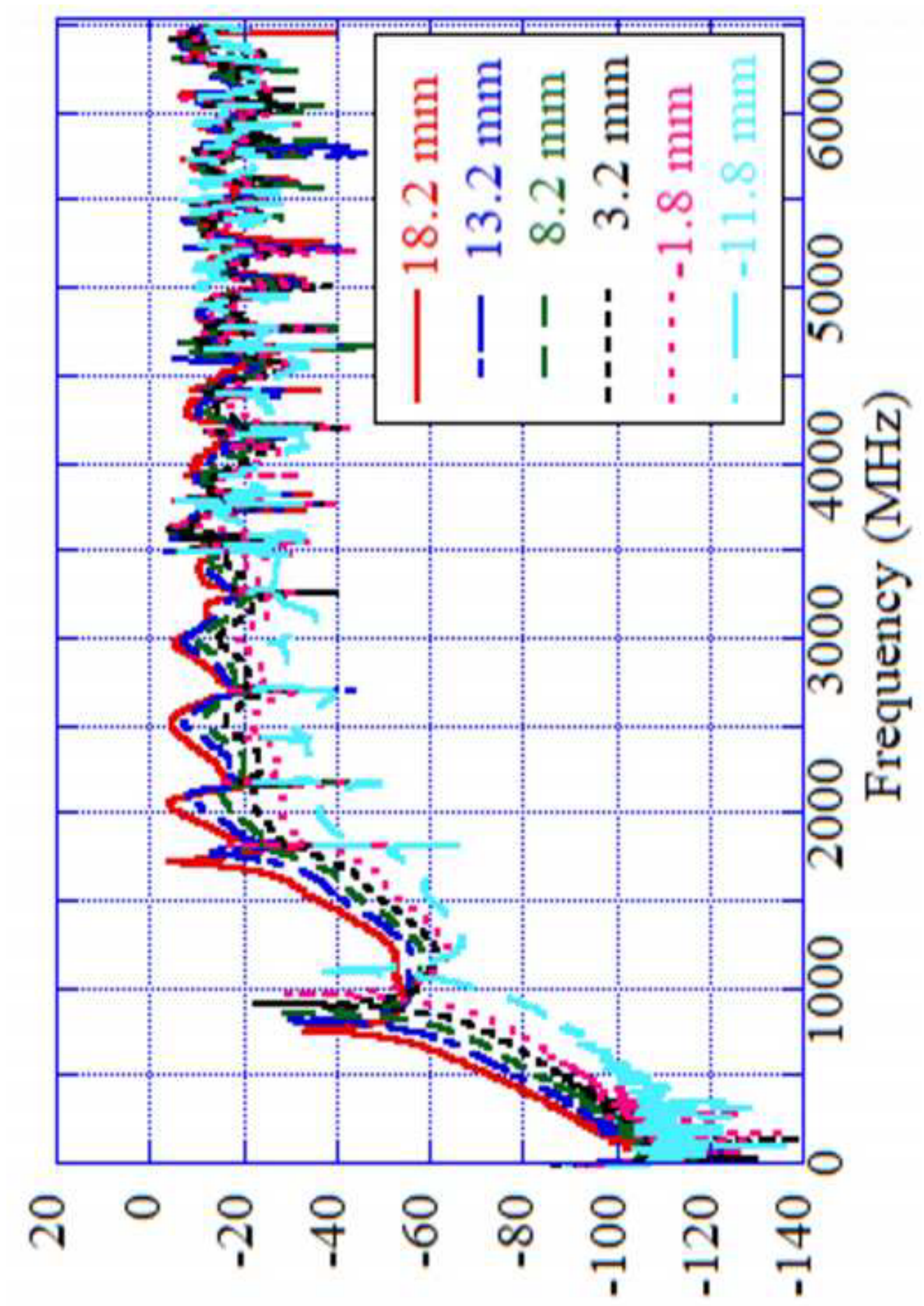
Transmission (dB)
Frequency (MHz)
18.2 mm
13.2 mm
8.2 mm
3.2 mm
-1.8 mm
-11.8 mm
20
0
-20
-40
-60
-80
-100
-120
-140
0
1000
2000
3000
4000
5000
6000

Figure

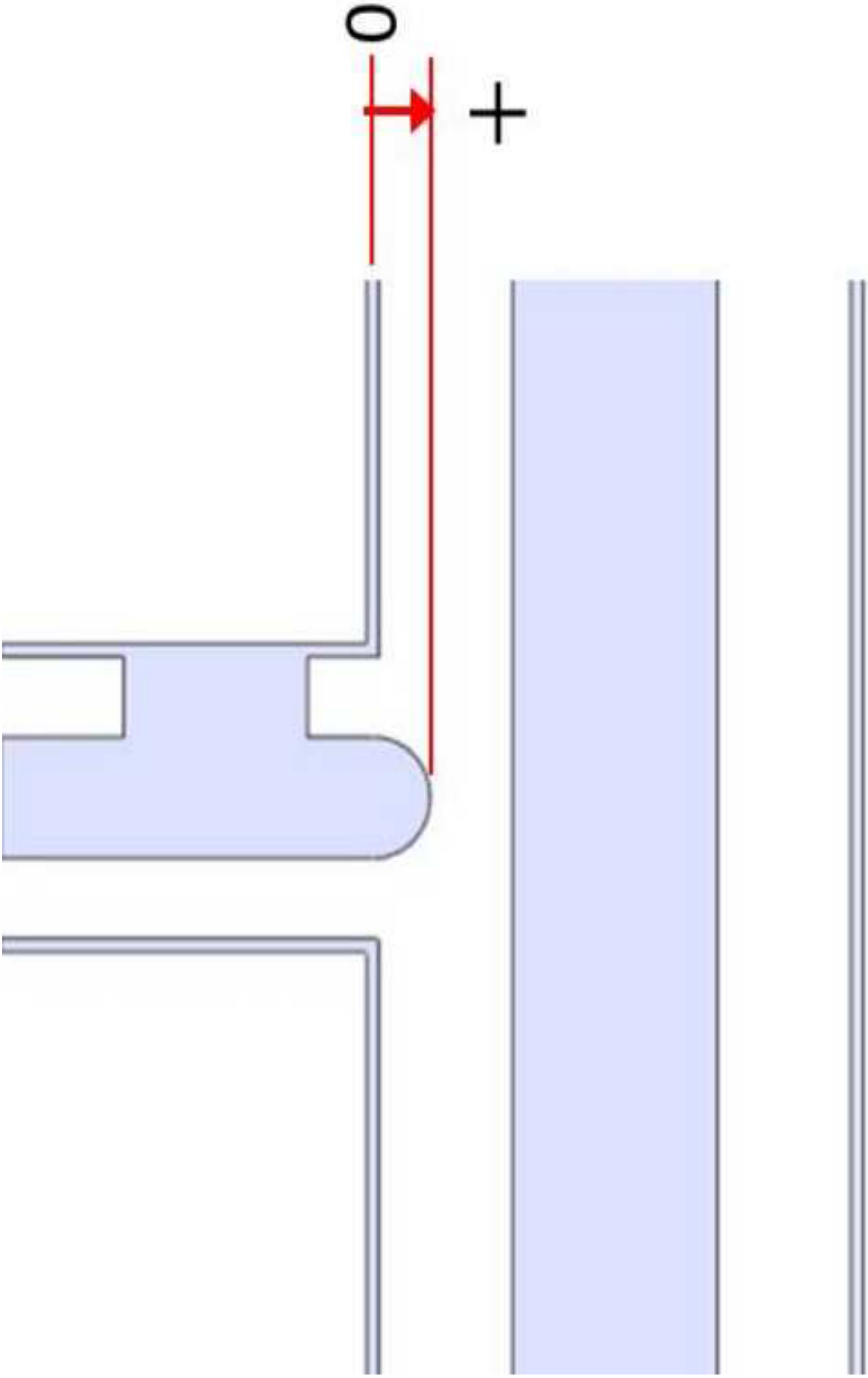

Figure

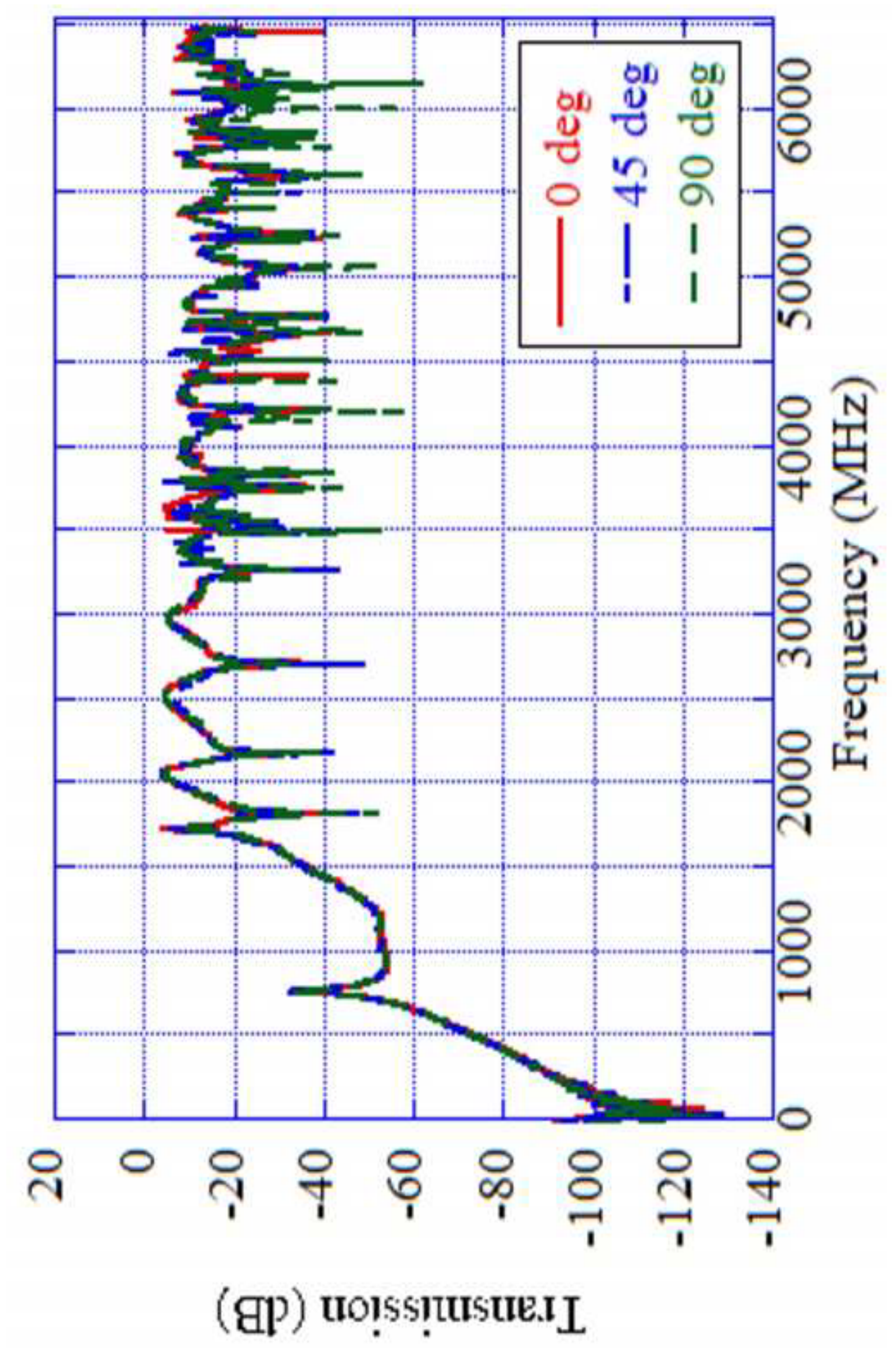
0 deg
45 deg
90 deg
Frequency (MHz)
Transmission (dB)
0
1000
2000
3000
4000
5000
6000
20
0
-20
-40
-60
-80
-100
-120
-140

Figure

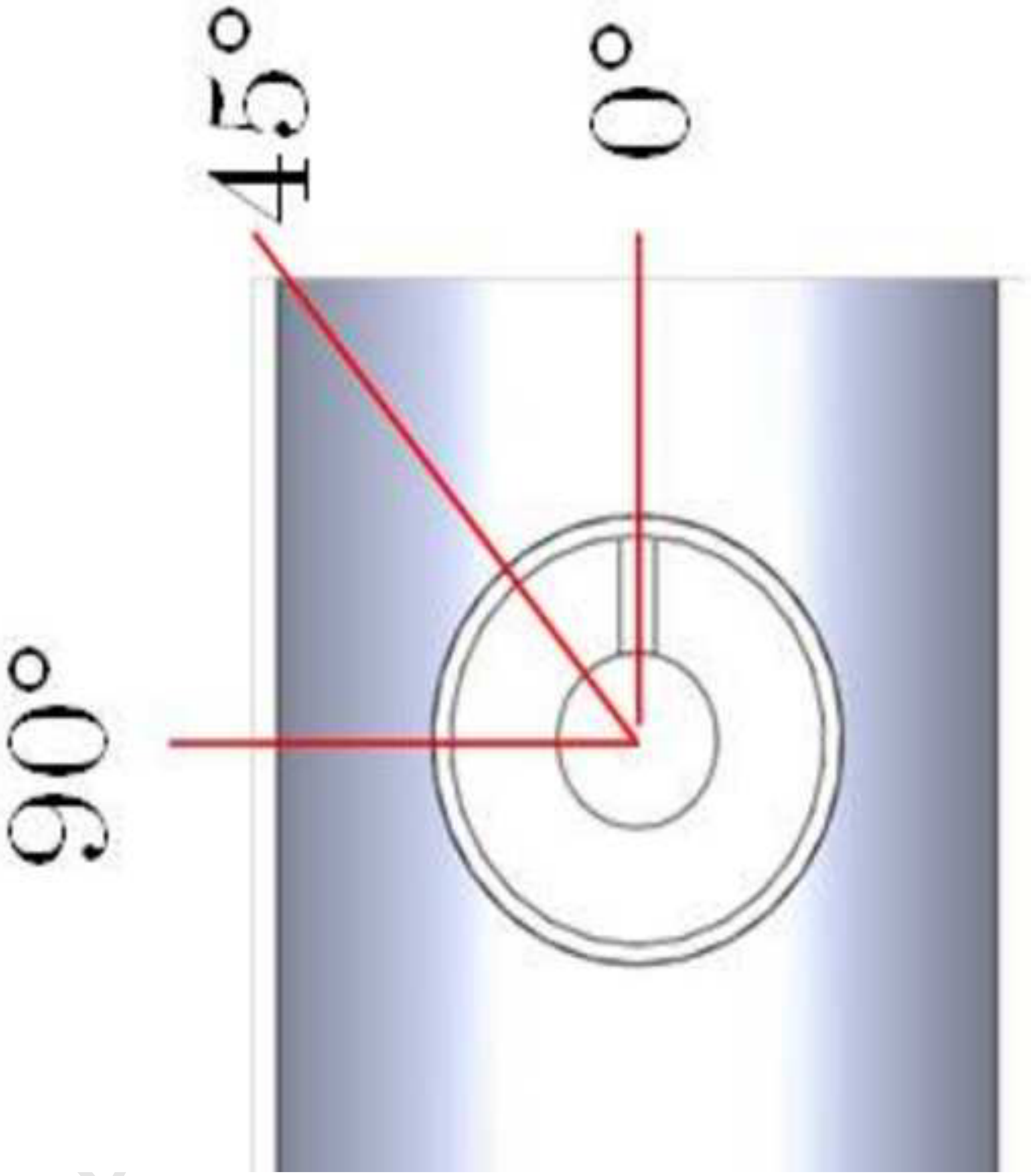

Figure

Figure

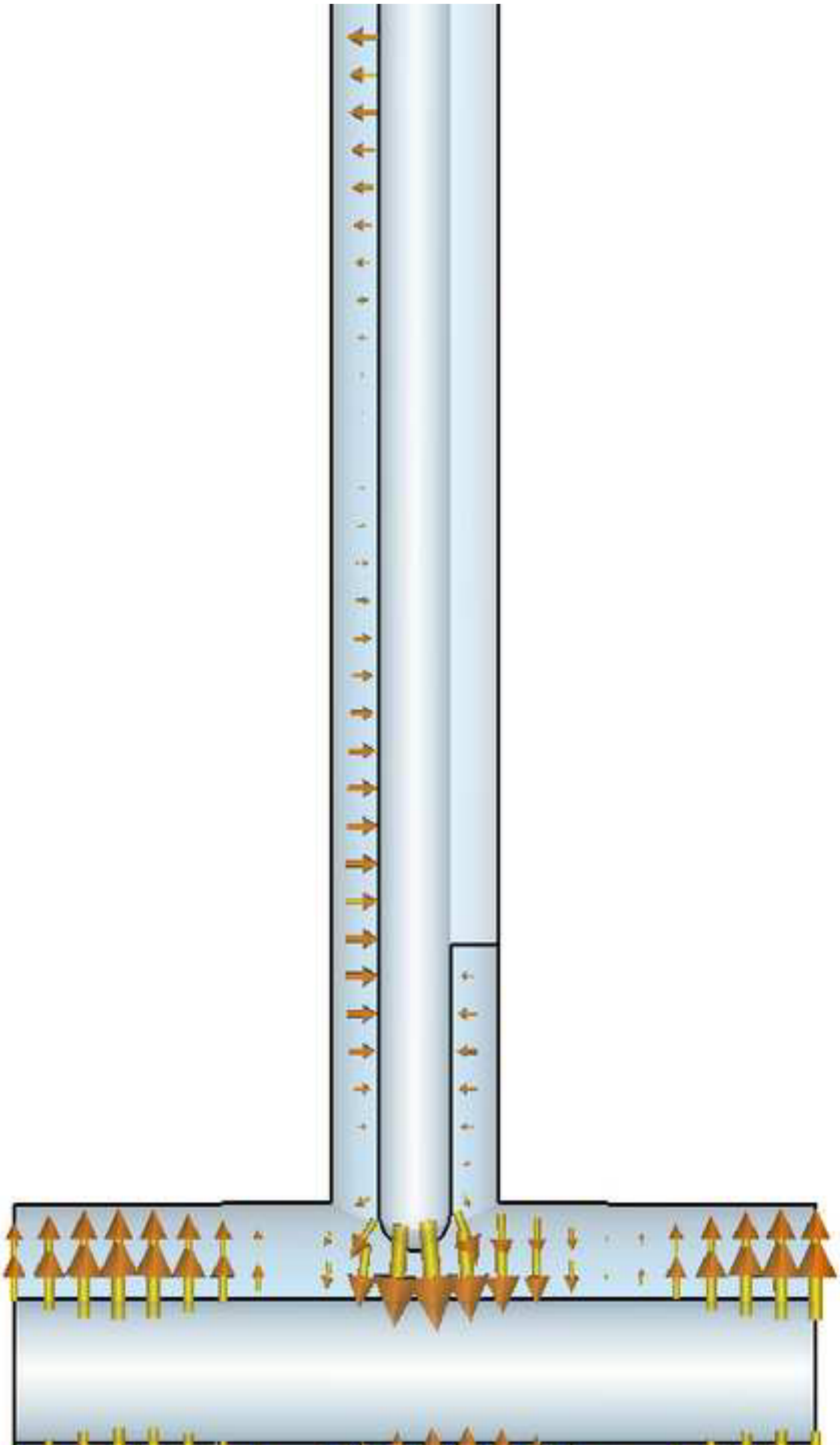

Figure

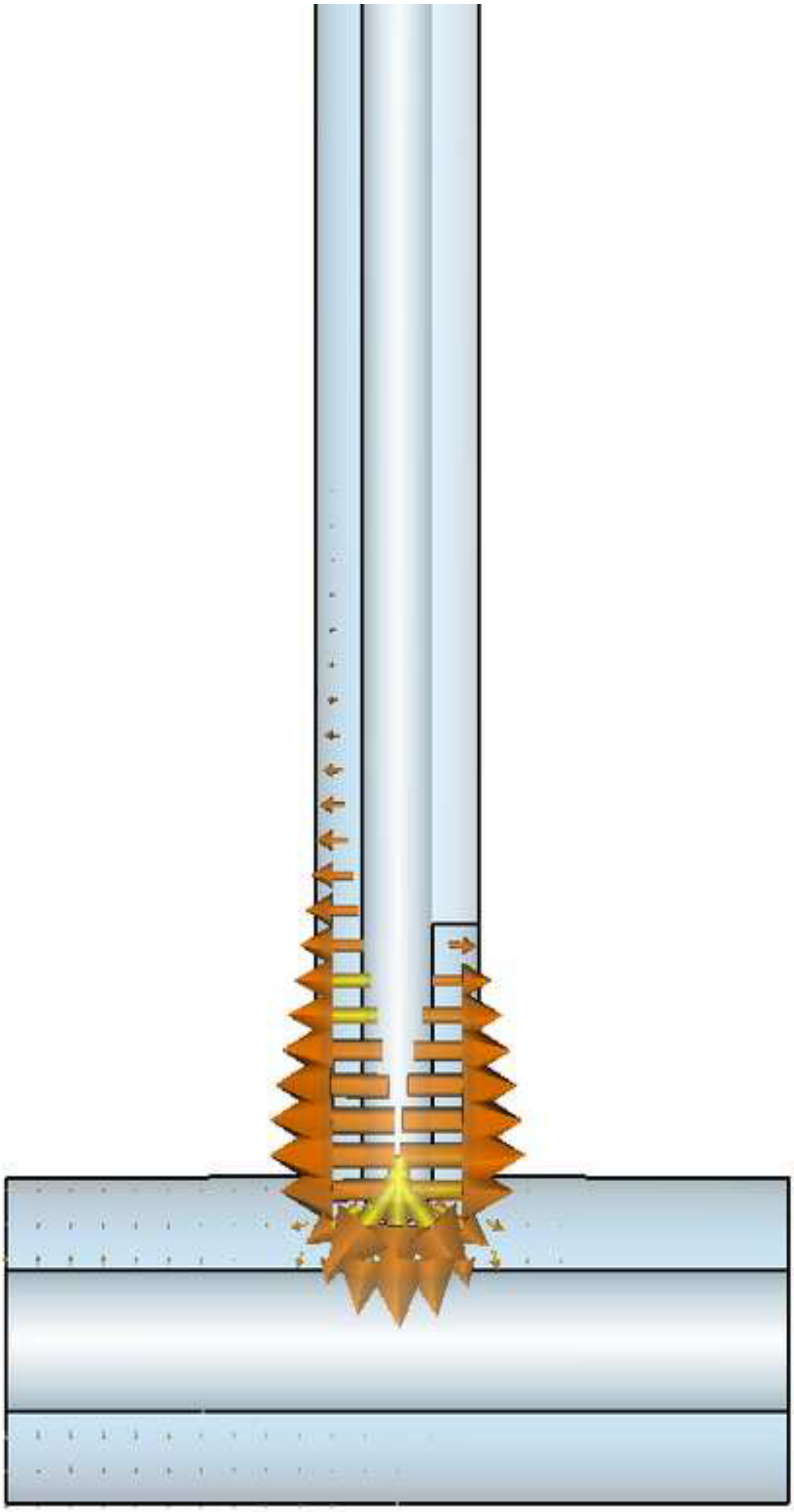

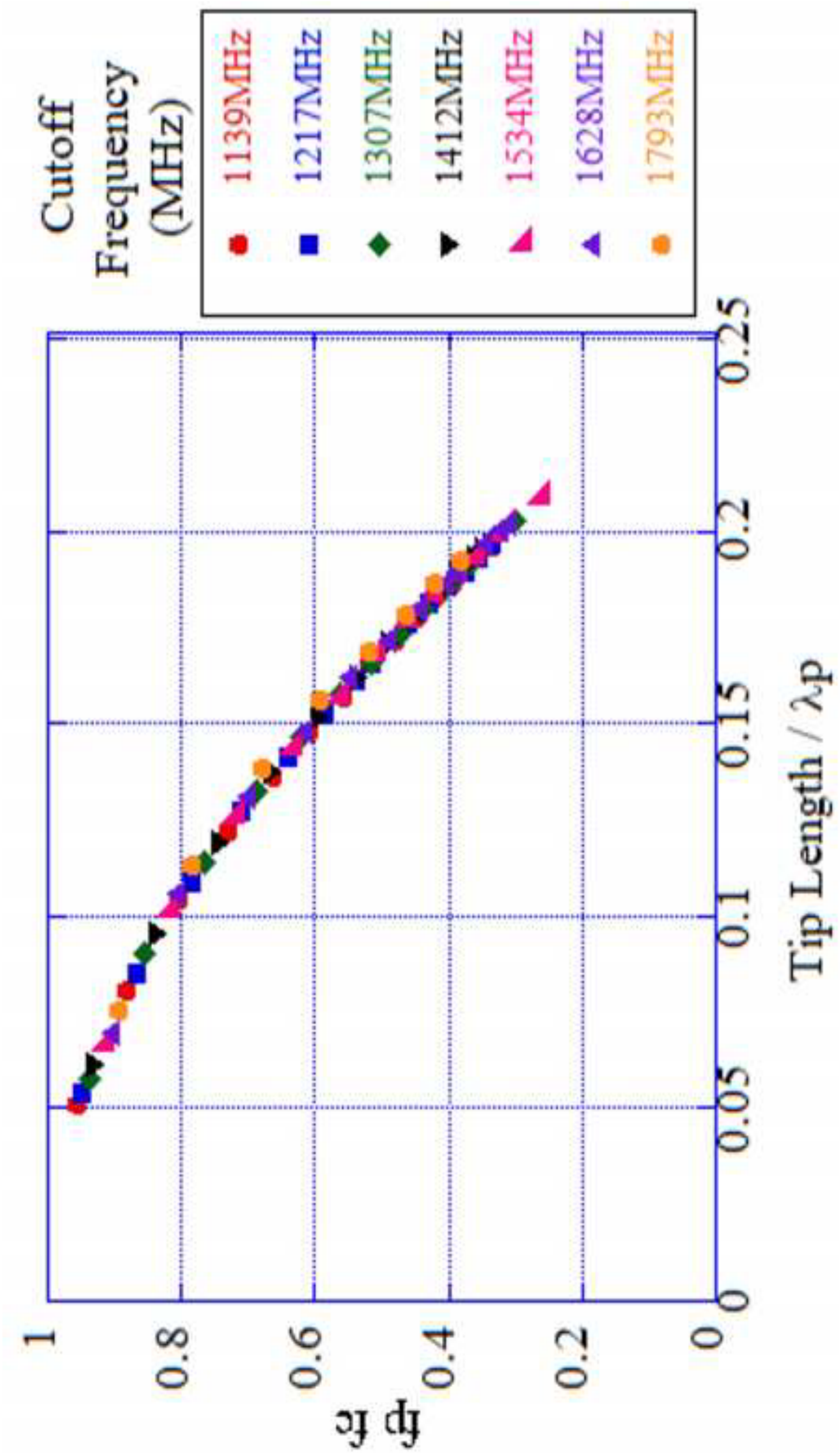
Cutoff Frequency (MHz)
1139MHz
1217MHz
1307MHz
1412MHz
1534MHz
1628MHz
1793MHz
fp fc
0
0.2
0.4
0.6
0.8
1
0
0.05
0.1
0.15
0.2
0.25
Tip Length / λp

Figure

Table 1 CSWG model parameters.

No.		1	2	3	4	5	6	7	8	9
Outer radius (mm)		21								
Inner radius (mm)		4.5	6	7.5	9	15	9			
Connection plate	Type	Parallel					Radial			
	Thickness (mm)	2					-----			
	Angle (deg)	-----					15	30	45	60
Length (mm)		65, 115, 165, 215 (total length from 65 to 560)								

Table 2 Comparison of the cutoff frequencies of the radial connection plate determined by analysis, approximation, measurement and calculation for various connection plate angles, and the difference from the analysis.

	Cutoff frequency (MHz)				Difference from the analysis (%)			
Connection plate angle	15°	30°	45°	60°	15°	30°	45°	60°
Analysis	1782.8	1958.7	2180.1	2444.2	-	-	-	-
Approximation	1736.2	1909.9	2122.1	2387.3	-2.6	-2.5	-2.7	-2.3
Measurement	1797.0	1964.1	2205.6	2489.8	0.8	0.3	1.2	1.9
Calculation	1795.7	1973.3	2189.2	2459.7	0.7	0.7	0.4	0.6

Table 3 Comparison of the cutoff frequencies of the parallel connection plate determined by approximation, measurement and calculation for various inner conductor radii, and the difference from the calculation.

	Cutoff frequency (MHz)				Difference from the calculation (%)			
Inner conductor radius (mm)	4.5	6	7.5	9	4.5	6	7.5	9
Approximation	1970.8	1855.9	1753.7	1662.1	-6.8	-7.0	-3.8	-4.0
Measurement	2142.3	1970.3	1838.5	1721.6	1.3	-1.3	0.9	-0.6
Calculation	2114.9	1995.5	1822.1	1732.0	-	-	-	-